IEEE Access
Multidisciplinary ⋮ Rapid Review ⋮ Open Access Journal

Received 13 May 2024, accepted 1 July 2024, date of publication 8 July 2024, date of current version 16 July 2024.

*Digital Object Identifier 10.1109/ACCESS.2024.3424463*

RESEARCH ARTICLE

# Robust Finite-Time Adaptive Nonlinear Control System for an EOD Robotic Manipulator: Design, Implementation, and Experimental Validation

**LUIS F. CANAZA CCARI[1], WALKER AGUILAR[1], ELVIS SUPO[1], ERASMO SULLA ESPINOZA[1], YURI SILVA VIDAL[2], NICOLÁS MEDINA[1], AND LIZARDO PARI[1]**

[1]Electronic Engineering Professional School, Universidad Nacional de San Agustín de Arequipa, Arequipa 04000, Peru
[2]Mechanical Engineering Professional School, Universidad Nacional de San Agustín de Arequipa, Arequipa 04000, Peru

Corresponding author: Luis F. Canaza Ccari (lcanazacc@unsa.edu.pe)

The project has been funded by the Programa Nacional de Investigación Científica y Estudios Avanzados (PROCIENCIA) through CONTRACT No PE501079565-2022 signed between Universidad Nacional de San Agustín de Arequipa and PROCIENCIA.

**ABSTRACT** To improve the efficiency of human-robot interaction (HRI) in hazardous ordnance manipulation tasks, the design of an advanced control system for a robotic manipulator needs to be investigated. This article presents a robust finite-time adaptive nonlinear control system designed to address the trajectory tracking control of explosive ordnance disposal (EOD) robotic manipulator, considering the actuator dynamics and subject to external disturbances and uncertainties. First, the theoretical design of the controller is developed. In order to achieve fast convergence, high tracking accuracy, and strong robustness, which are fundamental features in EOD applications, a Backstepping Fast Terminal Sliding Mode Control (BFTSMC) strategy is proposed. The sliding surface coefficients are adaptively tuned in real-time by a neural network, where the backpropagation algorithm updates the neural network weight. The combination of the BFTSMC strategy and the adaptive neural network scheme results in the Adaptive Backstepping Fast Terminal Sliding Mode Control (ABFTSMC) strategy, achieving improved control system performance. The stability of the closed-loop control system is demonstrated using Lyapunov theory to guarantee the convergence of tracking errors to the origin in finite time. Next, a detailed description of the hardware system, encompassing sensors, actuators, and controller boards, is provided for the practical implementation of the ABFTSMC strategy. Finally, the proposed control system is experimentally validated through several tests on a real EOD robotic manipulator, and an extensive comparison analysis with other control approaches is performed. The results evidence that the ABFTSMC strategy demonstrates high robustness, fast convergence in finite time, and good tracking accuracy, which are crucial qualities in real-world EOD applications.

**INDEX TERMS** EOD manipulator, nonlinear control system, backstepping, sliding mode control.

## I. INTRODUCTION

### A. CONTEXT AND MOTIVATIONS FOR THE STUDY

Robotic manipulators are mechanical systems with several links, giving them greater flexibility and versatility to operate in various environments and perform specific tasks [1], [2]. Due to these capabilities, robotic manipulators have widespread applications in a variety of fields, such as the automotive industry [3], [4], surgical technology [5], [6], high-risk environments [7], [8], and many others.

Explosive ordnance disposal (EOD) represents a high-risk environment for EOD technicians, who are confronted with highly explosive packages in the course of their duties [9]. To improve technician safety in this context, using robotic manipulators in EOD tasks has proven crucial [10], [11], [12]. This robotic technology allows specialists to

The associate editor coordinating the review of this manuscript and approving it for publication was Mou Chen.

© 2024 The Authors. This work is licensed under a Creative Commons Attribution 4.0 License.
For more information, see https://creativecommons.org/licenses/by/4.0/

operate remotely, thus reducing their exposure to potentially fatal situations. However, to achieve effective human-robot interaction (HRI) in EOD manipulation tasks, it is essential to implement an efficient control system with robust trajectory tracking capability for EOD robotic manipulators. The control of an EOD robotic manipulator carries specific requirements [13], [14]. First, high accuracy is required to handle potentially explosive packages safely. In addition, a fast response is crucial so that the manipulator can react nimbly to unexpected events. Strong robustness is also demanded to allow the manipulator to adapt and recover from external disturbances, such as payload variations. These requirements are fundamental to ensure efficiency and safety in handling explosive ordnance by robotic manipulators. Therefore, it is necessary to investigate the design of advanced control strategies for implementation in EOD robotic manipulator control systems that provide high accuracy, fast response, and solid robustness. However, incorporating all these features into a single real hardware control system represents a considerable challenge for academics and researchers. This is due to the inherent complexity in modelling the dynamics of robotic manipulators, which includes factors such as actuator dynamics, dynamic coupling effects, time-varying nonlinear parameters, as well as external disturbances and uncertainties to which robotic manipulators are exposed [15], [16], [17].

This article investigates the design, practical implementation on real hardware, and experimental validation of a robust finite-time control system to address the previously mentioned challenges to achieve trajectory tracking control of an EOD robotic manipulator. Therefore, the main objective of this research is to develop an advanced nonlinear control system that will be experimentally validated on an EOD robotic manipulator, aiming to simultaneously achieve high tracking accuracy, fast convergence, and strong robustness, all integrated into the same control system.

### B. LITERATURE REVIEW ON THE CONTROL OF ROBOTIC MANIPULATORS

In the literature, several research studies have been reported that focus on the control of robotic manipulators using different techniques, such as Proportional Integral Derivative (PID) control [18], [19], adaptive control [20], [21], intelligent control [22], [23], Backstepping control [24], [25], and Sliding Mode Control [26], [27]. Sliding Mode Control (SMC) is a robust nonlinear control strategy widely used in the literature to address trajectory tracking control of robotic systems with complex dynamics [28], [29], [30]. This is due to its simple design and ability to deal with modelling uncertainties and external disturbances. However, conventional sliding mode control experiences a phenomenon known as chattering, which degrades the controller performance by introducing high frequencies into the control input signal [31]. This chattering can cause instability in the EOD robotic manipulator and irreversibly damage its motors. Several advanced control strategies have been proposed for trajectory tracking in robotic manipulators to overcome this limitation. In [32], the authors presented an adaptive sliding mode controller for controlling a serial manipulator, which uses fuzzy logic to compensate for the high-frequency terms of the uncertainties. Also, in [33], an adaptive sliding mode control, but with a Nussbaum function, was used to control a 3-degree-of-freedom (DoF) robotic manipulator. On the other hand, research [34] proposed a continuous sliding mode controller and employed an observer to estimate time-varying external disturbances. Although these proposals solve the chattering problem associated with conventional sliding mode control, the proposed controllers achieved asymptotic stability, i.e., they achieve a slow convergence rate of the robotic manipulator states. This makes them less suitable for practical high-precision applications, such as those related to EOD, where the priority is to achieve fast convergence. Modern control strategies with finite-time stability have been introduced in the literature to address this limitation, which aims to improve control performance and achieve fast convergence in robotic manipulator trajectory tracking.

The work [35] proposed a second-order terminal sliding mode adaptive controller to control a 2 DoF robotic manipulator. Based on this proposal, [36], [37] presented fast terminal sliding mode control strategies using neural networks to estimate the unknown uncertainties of 3 DoF [36] and 2 DoF [37] robotic manipulators, respectively. Research [38], [39] addressed the design of adaptive controllers using a non-singular fast terminal sliding mode control approach. In [38], a neural network was incorporated for uncertainty estimation, while in [39], adaptive laws are used for the same purpose. On the other hand, in the article [40], a non-singular fast terminal sliding mode control approach based on a finite-time disturbance observer was proposed to counteract external disturbances. It is important to note that the works [38], [39], [40] focused exclusively on trajectory tracking control for 2 DoF manipulators. On the other hand, to improve control robustness against external disturbances and parametric uncertainties, strategies combining backstepping and sliding mode techniques have been developed in the literature to achieve robust control in trajectory tracking for robotic manipulators [41], [42], [43]. In [41], a robust adaptive backstepping sliding mode controller for a 2 DoF manipulator was presented; however, finite-time control stability was not achieved. To address this deficiency, articles [42] and [43] presented a backstepping fast terminal sliding mode control strategy for a 2 DoF [42] and 3 DoF [43] robotic manipulator, respectively.

In previous research [32], [33], [34], [35], [36], [37], [38], [39], [40], [41], [42], [43], various advanced control strategies were employed for trajectory tracking of robotic manipulators, achieving promising results. However, it is essential to note that these studies were limited exclusively to results from numerical simulations, lacking experimental tests in a real hardware configuration. This restriction prevents the practical validation of the theoretical findings of the controllers in

practical situations. In addition, most of these works focused only on controlling 2 DoF robotic manipulators, simplifying the control compared to manipulators with more degrees of freedom. In addition, it is important to note that actuator dynamics was excluded in the control design in most of these works, unlike [38], which considered actuator dynamics. This is significant since actuator dynamics play a crucial role in the dynamic behaviour of the robotic manipulator. In contrast, our study presents a comprehensive control methodology, encompassing theoretical design, practical implementation, and experimental validation of a robust finite-time adaptive nonlinear control system for trajectory tracking of a 3 DoF robotic manipulator, including actuator dynamics. Although interesting works [44], [45], [46], [47] provided experimental results for trajectory tracking control of robotic manipulators, the following observations are raised: (i) They employed conventional sliding surfaces, i.e., linear surfaces that, according to sliding mode control theory [56], present the chattering phenomenon. (ii) The controllers presented asymptotic stability, i.e., they did not achieve fast finite-time convergence of the tracking errors to the origin. (iii) They focused on controlling 2 DoF manipulators, unlike the work [46], that addressed a 3 DoF manipulator.

### C. RELATED WORK

A PID control scheme has controlled most EOD robotic manipulators in real-world applications [48], [49], [50]. This is mainly due to the simplicity of the PID control design, which does not require detailed knowledge of the robotic manipulator dynamics and actuator dynamics [17]. In this way, PID control provides a simple and efficient solution to many control problems in real-world robotic manipulators. However, the use of PID controllers presents fundamental limitations for EOD robotic manipulators that should be mentioned: 1) In challenging EOD environments, with the presence of external disturbances and variability in the dynamic parameters of the robotic manipulator, PID control does not incorporate robustness against unknown disturbances and uncertainties, which could affect its performance. 2) PID control has asymptotic stability, achieving a slow convergence rate over time. This affects its performance in emergency situations, requiring fast and robust responses to abrupt changes. 3) PID control does not achieve high tracking accuracy, a crucial aspect in EOD environments requiring high precision. To the best of our knowledge, the existing literature has not addressed the design and practical implementation in real hardware of an advanced nonlinear control system for trajectory tracking of an EOD robotic manipulator. Although articles [51], [60] designed sliding mode control strategies for an EOD robotic manipulator, it is important to note that these works employed a linear sliding surface (conventional). As previously mentioned, using a linear sliding surface, despite achieving asymptotic stability, leads to the phenomenon of chattering. This phenomenon could lead to instabilities in the EOD robotic manipulator and cause irreversible damage to its motors. Moreover, the studies [51], [60] focused only on numerical simulations and did not address practical implementation and experimental validation on a real EOD robotic manipulator.

A fundamental conclusion derived from the analysis of previous research is the imperative need for further studies focused on controlling EOD robotic manipulators. Given the importance and increasing relevance of advanced nonlinear control techniques with finite time convergence, it is imperative to carry out research with experimental results to determine which control strategies are most appropriate in the practical operation of EOD robotic manipulators. Experimental investigations are highly recommended, as they contribute significantly to closing the gap between theoretical findings and their practical application through experimental validation, which is the main objective of this research.

### D. CONTRIBUTIONS

The main contributions of this research are as follows:

- In contrast to control approaches based on sliding mode theory [32], [33], [34], [35], [36], [37], [38], [39], [40], in this research, we have fused advanced nonlinear control techniques to develop a robust finite-time control strategy called Adaptive Backstepping Fast Terminal Sliding Mode Control (ABFTSMC). In addition, we have implemented an adaptive neural network scheme to dynamically tune the sliding surface coefficients in real-time, aiming to minimize the tracking errors in the face of unknown uncertainties and thus mitigate the effects of chattering.
- In contrast to works that have achieved asymptotic stability in experimental results [44], [45], [46], [47], the control strategy proposed in this research, ABFTSMC, ensures stability in finite time. This translates into fast convergence of the robotic manipulator states to the reference trajectory, high tracking accuracy, and solid robustness to external disturbances and uncertainties.
- Compared to finite-time control approaches [35], [36], [37], [38], [39], [40], [42], [43] that are limited to numerical simulation results, this research comprehensively addresses the theoretical design, practical implementation on real hardware, and experimental validation of the proposed control system ABFTSMC on a real robotic manipulator. To the best of our knowledge, this is the first time in the literature that such a comprehensive approach, from design to experimental validation, of an advanced nonlinear control with finite time stability applied to the control of an EOD robotic manipulator is performed.

In Table 1 compares the proposed ABFTSMC strategy with various control approaches in the literature.

### E. MANUSCRIPT ORGANIZATION

In Section II presents the preliminaries that will be used in the development of the article. In Section III deals with the

**TABLE 1. Comparison of control approaches for robotic manipulators.**

| Reference | Control strategy | Method for handling external disturbances and uncertainties | Type of stability | Degrees of freedom | Practical implementation | Experimental Validation | EOD Application |
|---|---|---|---|---|---|---|---|
| [36] | Fast terminal sliding mode | Adaptive laws based on neural network | Finite time stability | 3 DoF | X | X | X |
| [39] | Non-singular fast terminal sliding mode | Adaptive laws | Finite time stability | 2 DoF | X | X | X |
| [40] | Non-singular fast terminal sliding mode | Disturbance observation | Finite time stability | 2 DoF | X | X | X |
| [42] | Backstepping fast terminal sliding mode | Robustness | Finite time stability | 2 DoF | X | X | X |
| [43] | Backstepping terminal sliding mode | Disturbance observation | Finite time stability | 3 DoF | X | X | X |
| [44] | Conventional sliding mode | Adaptive laws | Asymptotic stability | 2 DoF | X | ✓ | X |
| [46] | Conventional sliding mode | Adaptive laws based on a fuzzy system | Asymptotic stability | 3 DoF | ✓ | ✓ | X |
| [51] | Conventional sliding mode | Adaptive laws based on a fuzzy system | Asymptotic stability | 4 DoF | X | X | ✓ |
| Proposed control system | Backstepping fast terminal sliding mode | Adaptive laws based on neural network | Finite time stability | 3 DoF | ✓ | ✓ | ✓ |

dynamics of the robotic manipulator, including the dynamics of the actuators. In Section IV, the design of the proposed control system is described. The practical implementation of the control system is detailed in Section V. Experimental validation is addressed in Section VI. Finally, Sections VII and VIII present the limitations and future work, as well as the conclusions of the work.

## II. PRELIMINARIES

In this section some definitions and mathematical lemmas used in control design and finite time stability proof are presented.

*Definition 1:* [29] (Finite-time stability). Consider the nonlinear system:

$$\dot{x} = f(x), \quad x(0) = x_0, \tag{1}$$

where $x \in \mathbb{R}^n$, and the nonlinear function $f : D \to \mathbb{R}^n$ is continuous on an open neighborhood of the origin $D \subseteq \mathbb{R}^n$. The origin $x = 0$ is a finite-time global convergent equilibrium of the nonlinear system (1) if it is globally asymptotically stable, and there is an open neighbourhood $U \subseteq D$ of the origin and a function $T_x : U \setminus \{0\} \to (0, \infty)$ such that each solution $x(t, x_0)$ of the nonlinear system (1) starting from the initial point $x_0 \in U \setminus \{0\}$ is well defined for $t \in [0, T_x(x_0))$, and $\lim_{t \to T_x(x_0)} x(t, x_0) = 0$. $T_x(x_0)$ is defined as the function of the convergence time, i.e., the settling time (with respect to $x_0$). The origin is a finite-time stable equilibrium if it is finite-time convergent and Lyapunov stable. If $U = D = \mathbb{R}^n$, the origin is said to be a globally stable equilibrium in finite time.

*Lemma 1:* [53] Suppose there exists a continuous positive definite Lyapunov function $V(x(t)) : \mathbb{R}^n \to \mathbb{R}$, and its derivative satisfies:

$$\dot{V}(x) \leq -L_V V^{\Delta} + F_V, \tag{2}$$

where $L_V > 0, 0 < \Delta < 1$ and $F_V > 0$ are positive definite constants, then the origin of system (1) is stable in finite time for $\forall 0 < \varrho < 1$, when the settling time is given by:

$$T_f = \frac{1}{(1-\Delta)\varrho L_V}\left(V^{1-\Delta}(x(0)) - \left(\frac{F_V}{(1-\varrho)L_V}\right)^{\frac{1-\Delta}{\Delta}}\right). \tag{3}$$

*Lemma 2:* [54] The following Young's inequality is true for $x, y \geq 0$ and $p, q > 1$, such that $\frac{1}{p} + \frac{1}{q} = 1$:

$$xy \leq \frac{x^p}{p} + \frac{y^q}{q}. \tag{4}$$

*Lemma 3:* [55] For the real variables $\gamma_1$ and $\gamma_2$, and any given constants $u > 0$, $v > 0$, and $\kappa > 0$, the following inequality holds:

$$|\gamma_1|^u |\gamma_2|^v \leq \frac{u}{u+v}\kappa|\gamma_1|^{u+v} + \frac{u}{u+v}\kappa^{\frac{-u}{v}}|\gamma_1|^{u+v}. \tag{5}$$

Furthermore, based on Lemma 3, let $\gamma_1 = 1$, $\gamma_2 = \gamma$, $u = 1-\varsigma$, $v = \varsigma$ and $\kappa = \varsigma^{\frac{\varsigma}{1-\varsigma}}$ for $0 < \varsigma < 1$. Then, equation (5) becomes:

$$|\gamma|^{\varsigma} \leq (1-\varsigma)\varsigma^{\frac{\varsigma}{1-\varsigma}} + |\gamma|. \tag{6}$$

## III. DYNAMIC MODEL AND CONTROL OBJECTIVE

### A. DYNAMIC MODEL OF THE ROBOTIC MANIPULATOR WITH ACTUATORS

The dynamics of a manipulator of $n$ degrees of freedom can be expressed in Lagrangian form as follows [59]:

$$M(q)\ddot{q} + C(q,\dot{q})\dot{q} + G(q) + D = \tau, \tag{7}$$

where $q$, $\dot{q}$, and $\ddot{q} \in \mathbb{R}^n$ are the position, velocity, and acceleration vectors of the robotic manipulator, respectively. $M(q) \in \mathbb{R}^{n\times n}$ denotes the positive definite inertia matrix, $C(q,\dot{q}) \in \mathbb{R}^{n\times n}$ represents the centripetal and Coriolis matrix, $G(q) \in \mathbb{R}^n$ is the vector of gravitational forces due to gravity. $D \in \mathbb{R}^n$ represents the external disturbances, and $\tau \in \mathbb{R}^n$ represents the vector of input torques acting on each joint of the robotic manipulator.

*Remark 1:* In practical situations, the torque vector of the robotic manipulator $\tau$ is supplied by actuators, usually DC motors. In this context, the dynamics of the actuators driving the joints must be considered in the total dynamics of the manipulator [38].

The dynamics of a DC motor can be expressed as follows [52]:

$$\tau_m = J_m\ddot{q}_m + B_m\dot{q}_m + \tau_n, \tag{8}$$

where $q_m \in \mathbb{R}^n$ represents the angular position vector of the motors, $\tau_m \in \mathbb{R}^n$ represents the vector of torques developed by the motors, $J_m \in \mathbb{R}^{n\times n}$ denotes the diagonal matrix of the moments inertia of the motor shafts, $B_m \in \mathbb{R}^{n\times n}$ is a diagonal matrix of viscous friction coefficients of the motor shafts, and $\tau_n \in \mathbb{R}^n$ is the load torque vector on the motor shaft.

Since DC motors drive each joint of the robotic manipulator, we can obtain the relationship between the angular position of the manipulator $q$ and the angular position of the motor shaft $q_m$ with the following expression [17]:

$$g_r = \frac{q}{q_m} = \frac{\tau_n}{\tau}, \tag{9}$$

where $g_r \in \mathbb{R}^{n\times n}$ is a diagonal matrix representing the gear reduction ratio.

The torque developed by the DC motor is proportional to the armature voltage. Therefore, we obtain the following expression:

$$\tau_m = K_\tau u, \tag{10}$$

where $K_\tau \in \mathbb{R}^{n\times n}$ is a diagonal matrix of the DC motor torque constants, and $u \in \mathbb{R}^n$ denotes the armature voltage vector of the motors.

Substituting (8), (9), and (10) into (7), the complete dynamics of the robotic manipulator with actuators can be expressed as:

$$M_T(q)\ddot{q} + C_T(q,\dot{q})\dot{q} + G_T(q) + D_T = u, \tag{11}$$

where $M_T = K_\tau^{-1}(g_r M + g_r^{-1}J_m)$, $C_T = K_\tau^{-1}(g_r C + g_r^{-1}B_m)$, $G_T = K_\tau^{-1}g_r G$ y $D_T = K_\tau^{-1}g_r D$.

The complete dynamics of the manipulator with the actuator in (11) has the following properties:

*Property 1:* The matrix $M_T$ is bounded, symmetric, and positive definite, satisfying the following:

$$\zeta_1 \|x\|^2 \le x^T M_T(q)x \le \zeta_2 \|x\|^2, \forall\ x, q \in \mathbb{R}^n,$$

where $\zeta_1, \zeta_2$ are positive constants.

*Property 2:* The matrix $C_T(q,\dot{q})$ and the time derivative of $M_T(q)$ satisfy:

$$x^T[\dot{M}_T(q) - 2C_T(q,\dot{q})]x = 0, \forall\ x, q, \dot{q} \in \mathbb{R}^n.$$

Now, the dynamic model in (11) can be expressed as follows:

$$\ddot{q} = M_T(q)^{-1}\left[-C_T(q,\dot{q}) - G_T(q) - D_T + u\right]. \tag{12}$$

We define $x_1 = q \in \mathbb{R}^n$ and $x_2 = \dot{q} \in \mathbb{R}^n$; the dynamical model in (12) can be transformed into a second-order state-space model as follows:

$$\begin{aligned} \dot{x}_1 &= x_2, \\ \dot{x}_2 &= M_T(q)^{-1}\left[-C_T(q,\dot{q}) - G_T(q) - D_T + u\right], \\ y &= x_1, \end{aligned} \tag{13}$$

where $y = x_1 = q \in \mathbb{R}^n$ represents the outputs of the system, i.e., the angular positions of the robotic manipulator joints.

### B. CONTROL OBJECTIVE

The control objective of the present study is to develop a robust and reliable control system to address the trajectory tracking of an EOD robotic manipulator. Therefore, the control strategy must satisfy the following points:

- Ensure that the position tracking errors $e(t) = q_d(t) - q(t) \in \mathbb{R}^n$ converge to zero in finite time $T_f$, i.e:

$$\lim_{t\to T_f} e(t) = 0, \quad \forall t > T_f,$$

  where $q_d \in \mathbb{R}^n$ is the desired trajectory.
- The control system must ensure robustness and be able to adapt to external disturbances and uncertainties.
- Ensure finite time stability of the whole closed-loop control system.

## IV. CONTROL SYSTEM DESIGN

In this section, the ABFTSMC control system is developed to address the trajectory tracking of an EOD robotic manipulator subject to external disturbances and uncertainties. First, Backstepping [24] and Sliding Mode [26] control theories are integrated, combining both techniques to design the BFTSMC strategy. Subsequently, adaptive laws are designed to allow real-time tuning of the sliding surface coefficients by implementing an adaptive neural network scheme. Finally, an exhaustive verification is carried out to guarantee the finite time stability of the proposed control system.

### A. BFTSMC STRATEGY DESIGN

Considering the dynamical system in (13), we define the position tracking error $e_1 \in \mathbb{R}^n$ and its time derivative as:

$$\begin{aligned} e_1 &= q_d - q, \\ \dot{e}_1 &= \dot{q}_d - \dot{q}, \end{aligned} \tag{14}$$

where $q_d \in \mathbb{R}^n$ y $\dot{q}_d \in \mathbb{R}^n$ represent the desired position trajectory and the desired velocity, respectively, then, we define the first candidate Lyapunov function with its derivative as:

$$\begin{aligned} V_1 &= \frac{1}{2} e_1^T e_1, \\ \dot{V}_1 &= e_1^T \dot{e}_1 = e_1^T (\dot{q}_d - \dot{q}). \end{aligned} \tag{15}$$

To ensure the stability of the first candidate Lyapunov function in (15), i.e. $\dot{V}_1 \leq 0$, $\dot{q}$ is considered as the controlling term. Therefore, a virtual control input $\chi \in \mathbb{R}^n$ is chosen such that $\dot{q} = \chi$, and is defined as follows:

$$\chi = \dot{q}_d + \lambda e_1, \tag{16}$$

where $\lambda = \text{diag}(\lambda_1, \lambda_2, \ldots, \lambda_n)$ is a positive definite diagonal matrix with parameters $\lambda_i > 0$ for $i = 1, 2, \ldots, n$.

Considering the virtual input $\chi$, a new error variable is introduced described by:

$$e_2 = \chi - \dot{q} = \dot{q}_d + \lambda e_1 - \dot{q}. \tag{17}$$

The introduction of $e_2$ causes the time derivative of $V_1$ to become:

$$\begin{aligned} \dot{V}_1 &= e_1^T \left( \dot{q}_d - (\dot{q}_d + \lambda e_1 - e_2) \right) \\ &= -e_1^T \lambda e_1 + e_1^T e_2. \end{aligned} \tag{18}$$

Clearly, if $e_2 = 0$, one obtains $\dot{V}_1 = -e_1^T \lambda e_1 \leq 0$. Therefore, the time derivative of $e_2$ is expressed as:

$$\begin{aligned} \dot{e}_2 &= \ddot{q}_d + \lambda \dot{e}_1 - \ddot{q} \\ &= \ddot{q}_d + \lambda \dot{e}_1 - M_T(q)^{-1} \left[ -C_T(q, \dot{q}) - G_T(q) - D_T + u \right]. \end{aligned} \tag{19}$$

Considering the errors $e_1$ and $e_2$ and inspired by the work [56], the following fast terminal sliding surface is proposed as a function of the errors $e_1$ and $e_2$ as follows:

$$s = e_2 + \alpha e_1 + \beta |e_1|^{\delta} \text{sign}(e_1), \tag{20}$$

where $s = [s_1, s_2, \ldots, s_n]^T$ are the sliding surfaces, and $1 < \delta < 2$ is the control design parameter. Then $\alpha = \text{diag}(\alpha_1, \alpha_2, \ldots, \alpha_n)^T$ and $\beta = \text{diag}(\beta_1, \beta_2, \ldots, \beta_n)^T$ are positive definite diagonal matrices, which will be adaptively tuned with a neural network in the next subsection. The time derivative of (20) is expressed as:

$$\dot{s} = \dot{e}_2 + \alpha \dot{e}_1 + \beta \delta |e_1|^{\delta - 1} \dot{e}_1. \tag{21}$$

The control law required to achieve finite-time stability, high tracking accuracy, and robustness in the robotic manipulator is designed as follows:

$$u = M_T(q) \left[ u_{\text{eq}} + u_{\text{r}} \right], \tag{22}$$

where $u_{\text{eq}}$ represents the equivalent control term, and $u_{\text{r}}$ represents the reach control term.

*Remark 2:* The control term $u_{\text{r}}$ provides fast convergence of the system states to the sliding surface $s$, while the term $u_{\text{eq}}$ is responsible for maintaining the system states on the sliding surface $s = 0$.

To achieve fast convergence in finite time to the sliding surface, the reach control term is designed as follows:

$$u_{\text{r}} = \eta s + K \text{sign}(s), \tag{23}$$

where $\eta = \text{diag}(\eta_1, \eta_2, \ldots, \eta_n)^T$ and $K = \text{diag}(K_1, \ldots, K_n)^T$ are positive definite diagonal matrices, which will be adaptively tuned with a neural network in the next subsection.

The equivalent control term $u_{\text{eq}}$ can be obtained from the sliding surface defined in (20). For this, a second candidate Lyapunov function is defined as:

$$V_2 = \frac{1}{2} s^T s. \tag{24}$$

The time derivative of (24) and substituting (19) is expressed as:

$$\begin{aligned} \dot{V}_2 =& s^T \dot{s} \\ =& s^T (\dot{e}_2 + \alpha \dot{e}_1 + \beta \delta |e_1|^{\delta - 1} \dot{e}_1) \\ =& s^T \big( \ddot{q}_d + \lambda \dot{e}_1 - M_T(q)^{-1} \big[ -C_T(q, \dot{q}) \\ & - G_T(q) - D_T + u \big] + \alpha \dot{e}_1 + \beta \delta |e_1|^{\delta - 1} \dot{e}_1 \big). \end{aligned} \tag{25}$$

The stability of the second candidate Lyapunov function (24) is guaranteed when the sliding manifold is reached, i.e., $s = \dot{s} = 0$. For this, in (25), we consider that $u = u_{\text{eq}}$. Therefore, the equivalent control term is designed as follows:

$$\begin{aligned} u_{\text{eq}} = & \ddot{q}_d + \lambda \dot{e}_1 + M_T(q)^{-1} C_T(q, \dot{q}) + M_T(q)^{-1} G_T(q) \\ & + M_T(q)^{-1} D_T + \alpha \dot{e}_1 + \beta \delta |e_1|^{\delta - 1} \dot{e}_1. \end{aligned} \tag{26}$$

Then, using (23) and (26), the final control law is designed as follows:

$$\begin{aligned} u = M_T(q) \Big[ & \ddot{q}_d + \lambda \dot{e}_1 + M_T(q)^{-1} C_T(q, \dot{q}) \\ & + M_T(q)^{-1} G_T(q) + M_T(q)^{-1} D_T + \alpha \dot{e}_1 \\ & + \beta \delta |e_1|^{\delta - 1} \dot{e}_1 + \eta s + K \text{sign}(s) \Big]. \end{aligned} \tag{27}$$

### B. ABFTSMC STRATEGY DESIGN

In this subsection, a neural network is implemented to adaptively tune the sliding surface parameters, such as $\alpha$, $\beta$, $\eta$, and $K$ in real-time. This adaptation aims to minimize tracking errors in the presence of unknown uncertainties and thereby mitigate the effects of chattering, enabling the effective performance of the control strategy designed in (27) under external disturbances and uncertainties. The neural network is trained using a specialized online learning architecture [57], [58], using the backpropagation algorithm to dynamically tune the parameters of the sliding surface

in each sample. For this purpose, the control law in (27) is modified as follows:

$$u = M_T(q)\Big[\ddot{q}_d + M_T(q)^{-1}C_T(q,\dot{q}) + M_T(q)^{-1}G_T(q) + M_T(q)^{-1}D_T + \dot{e}_1(\lambda + \widehat{\alpha}) + \widehat{\beta}\delta\,|e_1|^{\delta-1}\,\dot{e}_1 + \widehat{\eta}s + \widehat{K}\,\mathrm{sign}(s)\Big]. \tag{28}$$

Next, we design the parameters $\widehat{\alpha}, \widehat{\beta}, \widehat{\eta}, \widehat{K}$ by following the steps below:

1) First, we define the performance error $E_\theta$ as a function of the difference between the desired trajectory and the current position of the robotic manipulator.

$$E_\theta = \frac{1}{2}\big[q_d - q\big]^2. \tag{29}$$

2) Employing the steepest descent method [57], we derive the following adaptive equations:

$$\begin{aligned}
\widehat{K} &= K_0 - \omega\int_0^t \frac{\partial E_\theta}{\partial \widehat{K}}dt,\\
\widehat{\eta} &= \eta_0 - \omega\int_0^t \frac{\partial E_\theta}{\partial \widehat{\eta}}dt,\\
\widehat{\alpha} &= \alpha_0 - \omega\int_0^t \frac{\partial E_\theta}{\partial \widehat{\alpha}}dt,\\
\widehat{\beta} &= \beta_0 - \omega\int_0^t \frac{\partial E_\theta}{\partial \widehat{\beta}}dt,
\end{aligned} \tag{30}$$

where $\omega$ is the learning rate, and $K_0$, $\eta_0$, $\alpha_0$ and $\beta_0$ are initial values of $\widehat{K}$, $\widehat{\eta}$, $\widehat{\alpha}$ and $\widehat{\beta}$, respectively.

3) Using the chain rule for partial derivatives, we obtain:

$$\begin{aligned}
\frac{\partial E_\theta}{\partial \widehat{K}} &= \frac{\partial E_\theta}{\partial q}\frac{\partial q}{\partial u}\frac{\partial u}{\partial \widehat{K}} = -(e_1)\Theta M_a(q)\tanh(s),\\
\frac{\partial E_\theta}{\partial \widehat{\eta}} &= \frac{\partial E_\theta}{\partial q}\frac{\partial q}{\partial u}\frac{\partial u}{\partial \widehat{\eta}} = -(e_1)\Theta M_a(q)s,\\
\frac{\partial E_\theta}{\partial \widehat{\alpha}} &= \frac{\partial E_\theta}{\partial q}\frac{\partial q}{\partial u}\frac{\partial u}{\partial s}\frac{\partial s}{\partial \widehat{\alpha}}\\
&= -(e_1)^2\Theta M_a(q)\left(\widehat{\eta} + \frac{4e^{-2s}\widehat{K}}{(1+e^{-2s})^2}\right),\\
\frac{\partial E_\theta}{\partial \widehat{\beta}} &= \frac{\partial E_\theta}{\partial q}\frac{\partial q}{\partial u}\frac{\partial u}{\partial s}\frac{\partial s}{\partial \widehat{\beta}}\\
&= -(e_1)\Theta M_a(q)\left(\widehat{\eta} + \frac{4e^{-2s}\widehat{K}}{(1+e^{-2s})^2}\right)\mathrm{sign}^\delta(e_1),
\end{aligned} \tag{31}$$

where $\Theta = \mathrm{sign}\left(\frac{\Delta q}{\Delta u}\right)$. $\Delta$ is known as the ascending difference operator $\Delta\zeta_k = \zeta_k - \zeta_{k-1}$ [58].

4) Substituting (31) into (30), the adaptive parameters of the sliding surface are designed as:

$$\begin{aligned}
\widehat{K} &= K_0 + \omega\int_0^t\Big[(e_1)\Theta M_a(q)\tanh(s)\Big],\\
\widehat{\eta} &= \eta_0 + \omega\int_0^t\Big[(e_1)\Theta M_a(q)s\Big],\\
\widehat{\alpha} &= \alpha_0 + \omega\int_0^t\left[(e_1)^2\Theta M_a(q)\left(\widehat{\eta} + \frac{4e^{-2s}\widehat{K}}{(1+e^{-2s})^2}\right)\right],\\
\widehat{\beta} &= \beta_0 + \omega\int_0^t\left[(e_1)\Theta M_a(q)\left(\widehat{\eta} + \frac{4e^{-2s}\widehat{K}}{(1+e^{-2s})^2}\right)\cdot\mathrm{sign}^\delta(e_1)\right].
\end{aligned} \tag{32}$$

*Remark 3:* The adaptive laws designed in (32) and the control law designed in (28) result in an efficient and robust chattering-free control strategy to address the control of robotic manipulators. To the best of our knowledge, this is the first research work that develops and implements a nonlinear FTSMC strategy (28) with adaptive laws as established in (32) for the control of robotic manipulators, validated with experimental results on a real robotic manipulator.

In Fig. 1 presents the structure of the control system proposed in this research.

### C. FINITE TIME STABILITY ANALYSIS

This section investigates the finite-time stability of the closed-loop control system under the proposed control law. To analyze the stability, we consider the following theorem:

*Theorem 1:* Considering the dynamic model of a robotic manipulator system in the presence of external disturbances and uncertainties described by (11) and under the control law design according to (28) together with the adaptive laws designed in (32), the closed-loop control system is stable in finite time. This implies that the tracking errors converge to zero in finite time and are constantly maintained in a small region around the origin.

*Proof 1:* The proof of Theorem 1 consists of two steps: **1) Convergence during the reaching phase:** It is proved that the reaching time is bounded, i.e., the trajectories of the robotic manipulator states reach the sliding surface in a finite time $T_r$. **2) Convergence during the sliding phase:** After reaching the sliding surface, it is proved that all signals within the closed-loop control system are bounded and that the trajectories of the robotic manipulator states converge to the equilibrium point in finite time $T_s$.

- **Step 1.** By recalling the expression of $\dot{s}$ in (21) and substituting the expression of $\dot{e}_2$ in (19) into (21), we obtain the following:

$$\dot{s} = \ddot{q}_d + \lambda\dot{e}_1 - M_T(q)^{-1}\big[-C_T(q,\dot{q}) - G_T(q) - D_T + u\big] + \alpha\dot{e}_1 + \beta\delta\,|e_1|^{\delta-1}\,\dot{e}_1. \tag{33}$$

By substituting the control law in (22) into (33), the following is obtained:

$$\begin{aligned}
\dot{s} &= \ddot{q}_d + \lambda\dot{e}_1 - M_T(q)^{-1}\big[-C_T(q,\dot{q}) - G_T(q)\\
&\quad - D_T + M_T(q)\big(u_{\mathrm{eq}} + u_{\mathrm{r}}\big)\big] + \alpha\dot{e}_1 + \beta\delta\,|e_1|^{\delta-1}\,\dot{e}_1\\
&= \ddot{q}_d + \lambda\dot{e}_1 - M_T(q)^{-1}\big[-C_T(q,\dot{q}) - G_T(q)\\
&\quad - D_T + M_T(q)\big(\ddot{q}_d + \lambda\dot{e}_1 + M_T(q)^{-1}C_T(q,\dot{q})\\
&\quad + M_T(q)^{-1}G_T(q) + M_T(q)^{-1}D_T + \alpha\dot{e}_1
\end{aligned}$$

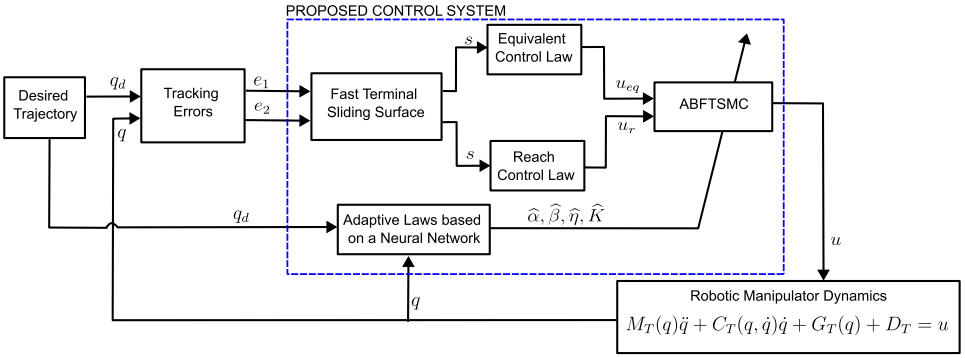


**FIGURE 1.** Structure of the proposed control system.

$$+ \beta\delta\,|e_1|^{\delta-1}\,\dot{e}_1 + u_r\big)\big] + \alpha\dot{e}_1 + \beta\delta\,|e_1|^{\delta-1}\,\dot{e}_1. \tag{34}$$

By performing some mathematical operations, we get:

$$\dot{s} = -u_r = -\eta s - K\,\mathrm{sign}(s). \tag{35}$$

By recalling the derivative of the second candidate Lyapunov function $V_2$ in (25) and substituting (35), we obtain the following:

$$\begin{aligned}\dot{V}_2 &= s(\dot{s})\\ &= s\big(-\eta s - K\,\mathrm{sign}(s)\big)\\ &= -\eta s^2 - K|s|.\end{aligned} \tag{36}$$

Considering (24), (36) can be rewritten as:

$$\begin{aligned}\dot{V}_2 &\le -2\eta\frac{s^2}{2} - \sqrt{2}K\left(\frac{s^2}{2}\right)^{1/2}\\ &\le -2\eta V_2 - \sqrt{2}K\left(V_2\right)^{\nabla},\end{aligned} \tag{37}$$

where $\nabla = 1/2$. Therefore, the trajectories of the robotic manipulator states reach the sliding surface in a finite time given by:

$$T_r = \frac{1}{2\eta(1-\nabla)}\ln\left[\frac{2\eta V_2^{1-\nabla}(0) + \sqrt{2}K}{\sqrt{2}K}\right]. \tag{38}$$

- **Step 2.** In this step, we prove that the tracking errors (14) and (17), the sliding surface (20), and the adaptive laws (32) will not lead the closed-loop system to instability and will converge to the equilibrium point in finite time. To achieve this, we define the following candidate Lyapunov function:

$$V = \frac{1}{2}e_1^2 + \frac{1}{2}e_2^2 + \frac{1}{2}s^2 + \frac{1}{2}\widetilde{K}^2 + \frac{1}{2}\widetilde{\eta}^2 + \frac{1}{2}\widetilde{\alpha}^2 + \frac{1}{2}\widetilde{\beta}^2, \tag{39}$$

where $\widetilde{K}, \widetilde{\eta}, \widetilde{\alpha}, \widetilde{\beta}$ are the adaptive estimation errors. Then $\widetilde{K} = \widehat{K} - K, \widetilde{\eta} = \widehat{\eta} - \eta, \widetilde{\alpha} = \widehat{\alpha} - \alpha, \widetilde{\beta} = \widehat{\beta} - \beta$. The time derivative (39) and substituting (14), (19), and (35), we obtain:

$$\begin{aligned}\dot{V} &= e_1\dot{e}_1 + e_2\dot{e}_2 + s\dot{s} + \widetilde{K}\dot{\widehat{K}} + \widetilde{\eta}\dot{\widehat{\eta}} + \widetilde{\alpha}\dot{\widehat{\alpha}} + \widetilde{\beta}\dot{\widehat{\beta}}\\ &= e_1(-\lambda e_1) + e_2(-\widehat{\alpha}\dot{e}_1 - \widehat{\beta}|e_1|^{\delta-1})\\ &\quad + s(-\widehat{\eta}s - \widehat{K}\,\mathrm{sign}(s)) + \widetilde{K}\dot{\widehat{K}} + \widetilde{\eta}\dot{\widehat{\eta}} + \widetilde{\alpha}\dot{\widehat{\alpha}} + \widetilde{\beta}\dot{\widehat{\beta}}.\end{aligned} \tag{40}$$

By performing mathematical operations and adding and subtracting the same terms, the result is obtained:

$$\begin{aligned}\dot{V} &= -\lambda e_1^2 - \widehat{\alpha}\dot{e}_1e_2 - \widehat{\beta}e_2|e_1|^{\delta-1} - \widehat{\eta}s^2 - \widehat{K}s\\ &\quad + \widetilde{K}\dot{\widehat{K}} + \widetilde{\eta}\dot{\widehat{\eta}} + \widetilde{\alpha}\dot{\widehat{\alpha}} + \widetilde{\beta}\dot{\widehat{\beta}} + \alpha\dot{e}_1e_2 - \alpha\dot{e}_1e_2\\ &\quad + \beta e_2|e_1|^{\delta-1} - \beta e_2|e_1|^{\delta-1} + \eta s^2 - \eta s^2 + Ks - Ks\\ &= -\lambda e_1^2 - \widetilde{\alpha}\dot{e}_1e_2 - \widetilde{\beta}e_2|e_1|^{\delta-1} - \widetilde{\eta}s^2 - \widetilde{K}s + \widetilde{K}\dot{\widehat{K}}\\ &\quad + \widetilde{\eta}\dot{\widehat{\eta}} + \widetilde{\alpha}\dot{\widehat{\alpha}} + \widetilde{\beta}\dot{\widehat{\beta}} - \alpha\dot{e}_1e_2 - \beta e_2|e_1|^{\delta-1} - \eta s^2 - Ks\\ &= -\lambda e_1^2 - \alpha\dot{e}_1e_2 - \beta e_2|e_1|^{\delta-1} - \eta s^2 - Ks\\ &\quad - (s - \dot{\widehat{K}})\widetilde{K} - (s^2 - \dot{\widehat{\eta}})\widetilde{\eta} - (\dot{e}_1e_2 - \dot{\widehat{\alpha}})\widetilde{\alpha} - (e_2|e_1|^{\delta-1} - \dot{\widehat{\beta}})\widetilde{\beta}\\ &= -\lambda e_1^2 - \alpha\dot{e}_1e_2 - \beta e_2|e_1|^{\delta-1} - \eta s^2 - Ks\\ &\quad - \rho_1\widetilde{K} - \rho_2\widetilde{\eta} - \rho_3\widetilde{\alpha} - \rho_4\widetilde{\beta},\end{aligned} \tag{41}$$

where $\rho_1 = (s - \dot{\widehat{K}})$, $\rho_2 = (s^2 - \dot{\widehat{\eta}})$, $\rho_3 = (\dot{e}_1e_2 - \dot{\widehat{\alpha}})$, $\rho_2 = (e_2|e_1|^{\delta-1} - \dot{\widehat{\beta}})$.

Applying Young's inequality according to Lemma 2, we derive the following expression:

$$\begin{aligned}\dot{V} \le &-2\lambda\left(\frac{e_1^2}{2}\right) - \alpha\left(\frac{\dot{e}_1^2 + e_2^2}{2}\right) - \beta\left(\frac{(|e_1|^{\delta-1})^2 + e_2^2}{2}\right)\\ &- 2\eta\left(\frac{s^2}{2}\right) - K\left(\frac{1+s^2}{2}\right) - \rho_1\left(\frac{1+\widetilde{K}^2}{2}\right)\\ &- \rho_2\left(\frac{1+\widetilde{\eta}^2}{2}\right) - \rho_3\left(\frac{1+\widetilde{\alpha}^2}{2}\right) - \rho_4\left(\frac{1+\widetilde{\beta}^2}{2}\right).\end{aligned} \tag{42}$$

By developing and ordering the expression (42), we can obtain the following:

$$\begin{aligned}\dot{V} \le &-2\lambda\left(\frac{e_1^2}{2}\right) - \alpha\left(\frac{(-\lambda e_1)^2}{2}\right) - \alpha\left(\frac{e_2^2}{2}\right)\\ &- \beta\left(\frac{|e_1|^{2(\delta-1)}}{2}\right) - \beta\left(\frac{e_2^2}{2}\right) - 2\eta\left(\frac{s^2}{2}\right) - \frac{K}{2}\\ &- K\left(\frac{s^2}{2}\right) - \frac{\rho_1}{2} - \rho_1\left(\frac{\widetilde{K}^2}{2}\right) - \frac{\rho_2}{2} - \rho_2\left(\frac{\widetilde{\eta}^2}{2}\right)\end{aligned}$$

$$
\begin{aligned}
&- \frac{\rho_3}{2} - \rho_3\left(\frac{\widetilde{\alpha}^2}{2}\right) - \frac{\rho_4}{2} - \rho_4\left(\frac{\widetilde{\beta}^2}{2}\right) \\
&\leq -(2\lambda+\alpha\lambda^2)\frac{e_1^2}{2} - (\alpha+\beta)\frac{e_2^2}{2} - \frac{2^{\delta-1}\beta}{2}\left(\frac{e_1^2}{2}\right)^{\delta-1} \\
&\quad - (2\eta+K)\frac{s^2}{2} - \rho_1\frac{\widetilde{K}^2}{2} - \rho_2\frac{\widetilde{\eta}^2}{2} - \rho_3\frac{\widetilde{\alpha}^2}{2} - \rho_4\frac{\widetilde{\beta}^2}{2} \\
&\quad - -\frac{K}{2} - \frac{\rho_1}{2} - \frac{\rho_2}{2} - \frac{\rho_3}{2} - \frac{\rho_4}{2}. \qquad (43)
\end{aligned}
$$

By making the change of variable $\Delta = \delta - 1$. The equation (43) can be expressed as:

$$
\begin{aligned}
\dot{V} \leq\ & -(2\lambda+\alpha\lambda^2)\frac{e_1^2}{2} - (\alpha+\beta)\frac{e_2^2}{2} - 2^{\Delta-1}\beta\left(\frac{e_1^2}{2}\right)^{\Delta} \\
& - (2\eta+K)\frac{s^2}{2} - \rho_1\frac{\widetilde{K}^2}{2} - \rho_2\frac{\widetilde{\eta}^2}{2} - \rho_3\frac{\widetilde{\alpha}^2}{2} - \rho_4\frac{\widetilde{\beta}^2}{2} \\
& - \frac{K}{2} - \frac{\rho_1}{2} - \frac{\rho_2}{2} - \frac{\rho_3}{2} - \frac{\rho_4}{2}. \qquad (44)
\end{aligned}
$$

Employing Lemma 3, the following inequality is satisfied:

$$
\begin{aligned}
\dot{V} \leq\ & -(2\lambda+\alpha\lambda^2)\left[\left(\frac{e_1^2}{2}\right)^{\Delta} - \Xi\right] - (\alpha+\beta)\left[\left(\frac{e_2^2}{2}\right)^{\Delta} - \Xi\right] \\
& - 2^{\Delta-1}\beta\left(\frac{e_1^2}{2}\right)^{\Delta} - (2\eta+K)\left[\left(\frac{s^2}{2}\right)^{\Delta} - \Xi\right] \\
& - \rho_1\left[\left(\frac{\widetilde{K}^2}{2}\right)^{\Delta} - \Xi\right] - \rho_2\left[\left(\frac{\widetilde{\eta}^2}{2}\right)^{\Delta} - \Xi\right] - \rho_3\left[\left(\frac{\widetilde{\alpha}^2}{2}\right)^{\Delta} - \Xi\right] \\
& - \rho_4\left[\left(\frac{\widetilde{\beta}^2}{2}\right)^{\Delta} - \Xi\right] - \frac{K}{2} - \frac{\rho_1}{2} - \frac{\rho_2}{2} - \frac{\rho_3}{2} - \frac{\rho_4}{2}, \qquad (45)
\end{aligned}
$$

where $\Xi = (1-\Delta)\Delta^{\frac{\Delta}{1-\Delta}}$.

By performing mathematical refinements and ordering the common terms, the inequality is stated as follows:

$$
\begin{aligned}
\dot{V} \leq\ & -(2\lambda+\alpha\lambda^2+2^{\Delta-1}\beta)\left(\frac{e_1^2}{2}\right)^{\Delta} + (2\lambda+\alpha\lambda^2)\Xi \\
& - (\alpha+\beta)\left(\frac{e_2^2}{2}\right)^{\Delta} + (\alpha+\beta)\Xi \\
& - (2\eta+K)\left(\frac{s^2}{2}\right)^{\Delta} + (2\eta+K)\Xi \\
& - \rho_1\left(\frac{\widetilde{K}^2}{2}\right)^{\Delta} + \rho_1\Xi - \rho_2\left(\frac{\widetilde{\eta}^2}{2}\right)^{\Delta} + \rho_2\Xi \\
& - \rho_3\left(\frac{\widetilde{\alpha}^2}{2}\right)^{\Delta} + \rho_3\Xi - \rho_4\left(\frac{\widetilde{\beta}^2}{2}\right)^{\Delta} \\
& + \rho_4\Xi - \frac{K}{2} - \frac{\rho_1}{2} - \frac{\rho_2}{2} - \frac{\rho_3}{2} - \frac{\rho_4}{2} \\
\leq\ & -\{2\lambda+\alpha\lambda^2+2^{\Delta-1}\beta\}\left(\frac{e_1^2}{2}\right)^{\Delta} - \{\alpha+\beta\}\left(\frac{e_2^2}{2}\right)^{\Delta} \\
& - \{2\eta+K\}\left(\frac{s^2}{2}\right)^{\Delta} - \{\rho_1\}\left(\frac{\widetilde{K}^2}{2}\right)^{\Delta} \\
& - \rho_2\left(\frac{\widetilde{\eta}^2}{2}\right)^{\Delta} - \{\rho_3\}\left(\frac{\widetilde{\alpha}^2}{2}\right)^{\Delta} \\
& - \{\rho_4\}\left(\frac{\widetilde{\beta}^2}{2}\right)^{\Delta} + \Big\{(2\lambda+\alpha\lambda^2+\alpha+\beta+2\eta+K)\Xi \\
& + (\rho_1+\rho_2+\rho_3+\rho_4)\Xi \\
& + \Big(-\frac{K}{2} - \frac{\rho_1}{2} - \frac{\rho_2}{2} - \frac{\rho_3}{2} - \frac{\rho_4}{2}\Big)\Big\} \\
\leq\ & -L_V V^{\Delta} + F_V, \qquad (46)
\end{aligned}
$$

where $L_V = \{2\lambda+\alpha\lambda^2+2^{\Delta-1}\beta, \alpha+\beta, 2\eta+K, \rho_1, \rho_2, \rho_3, \rho_4\}$ and $F_V = \{(2\lambda+\alpha\lambda^2+\alpha+\beta+2\eta+K+\rho_1+\rho_2+\rho_3+\rho_4)\Xi + \big(-\frac{K}{2} - \frac{\rho_1}{2} - \frac{\rho_2}{2} - \frac{\rho_3}{2} - \frac{\rho_4}{2}\big)\}$.

This analysis demonstrates that the candidate Lyapunov function defined in (39) gradually decreases, implying that $V \leq 0$. As a result, $V$ is bounded, ensuring that all signals in the system are bounded and do not diverge to infinity. Therefore, according to Lemma 1 and for any $0 < \varrho < 1$, the trajectories of the states of the robotic manipulator converge to the equilibrium point in a finite time given by:

$$
T_s = \frac{1}{(1-\Delta)\varrho L_V}\left(V^{1-\Delta}(0) - \left(\frac{F_V}{(1-\varrho)L_V}\right)^{\frac{1-\Delta}{\Delta}}\right). \qquad (47)
$$

Finally, the total time required for the closed-loop control system to achieve the desired stability in finite time, and hence the tracking errors $(e_1, e_2)$ to stabilize at zero equilibrium during the sliding motion $(s = 0)$, is given by $T_f = T_r + T_s$.

Thus, completing the proof. ■

## V. IMPLEMENTATION OF ABFTSMC STRATEGY

This section details the practical implementation of the proposed control system, ABFTSMC, on the EOD robotic manipulator of 5 DoF (see Fig. 2). Although the selected manipulator encompasses the base, shoulder, elbow, wrist, and gripper, we focus on the control of 3 DoF: the base, shoulder, and elbow, as these joints are crucial for performing various movements of the end-effector of the robotic manipulator.

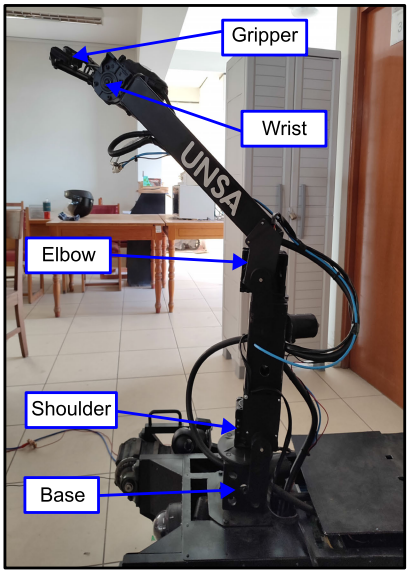


**FIGURE 2.** EOD robotic manipulator.

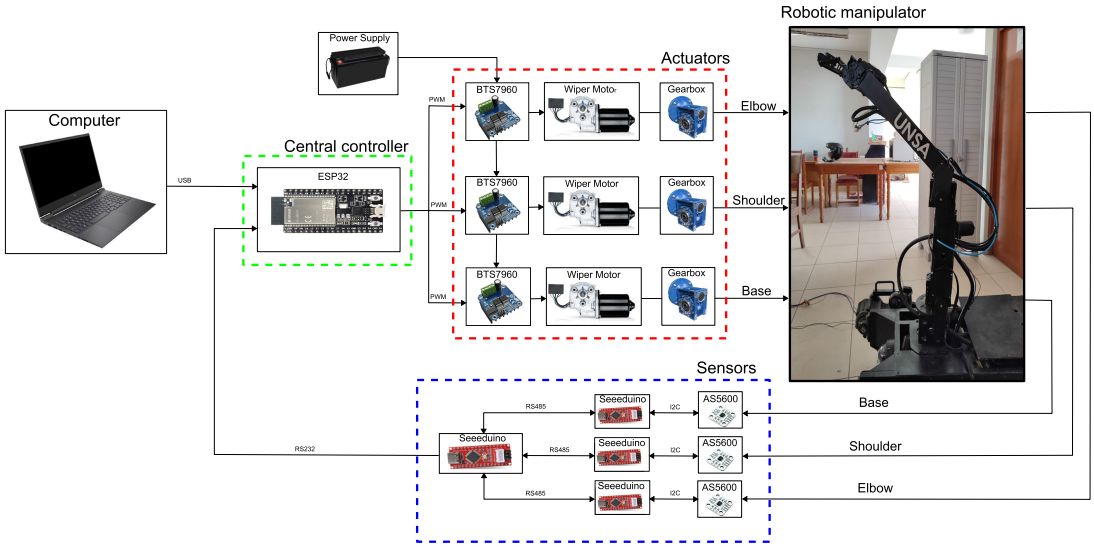


**FIGURE 3.** Connection of components for practical implementation.

In this study, we have chosen to employ 12V DC wiper motors as actuators for the robotic manipulator. These motors, known for their accessibility and low cost, offer a torque of 20 N.m., providing effective controllability for the EOD manipulator joints. To ensure high torque and precise manipulation, we have incorporated external worm gearboxes with a ratio of 20 (Rt=20), which also act as a brake. To obtain feedback on the angular position of the manipulator, we have implemented AS5600 magnetic encoders with 12-bit resolution, together with a Seeeduino development board for readout and data processing. To efficiently manage power, we have used BTS7960 H-bridge drivers, capable of tolerating up to 43 A peak. As the central controller, we selected the low-cost ESP32 microcontroller. The Fig. 3 illustrates the connection of these components with the real robotic manipulator, providing a detailed view of the implemented configuration.

According to Fig. 3, the reference signal is transmitted via a USB serial connection at 115200 baud to the central ESP32 controller. This controller runs the ABFTSMC algorithm and receives data from the angular positions of the base, shoulder, and elbow of the robotic manipulator through the AS5600 encoders. These encoders send the read data via the I2C communication protocol to the Seeduino development boards. In turn, this data is sent to a Seeduino leader development board via RS485 communication protocol for processing. The last processed data is transmitted to the ESP32 controller via an RS232 communication protocol. With this information and according to the reference signal, the leader controller sends pulse width modulation (PWM) signals to each BTS7960 H-bridge driver, which is in command of managing the direction of rotation of the wiper motors of each joint of the robotic manipulator.

## VI. EXPERIMENTAL VALIDATION

### A. EXPERIMENTAL SETUP

The ABFTSMC strategy was validated on an experimental setup, as shown in Fig. 4. This setup consists of several essential parts, including a robotic manipulator, a 12V power supply for the control system, a 24V battery for powering the robotic manipulator, an HP Victus Core i5 computer, and the control system. The physical parameters of the robotic manipulator and the control parameters associated with the ABFTSMC strategy are detailed in Tables 2 and 3, respectively.

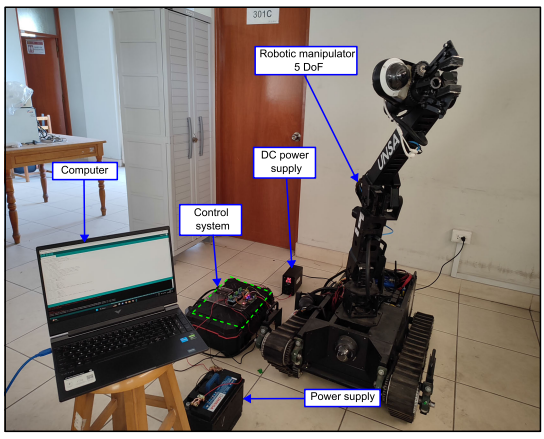


**FIGURE 4.** Experimental setup.

### B. EXPERIMENTAL RESULTS AND DISCUSSIONS

To validate the effectiveness of the proposed control system ABFTSMC, three experimental trajectory tracking tests were conducted on a real EOD robotic manipulator in a laboratory

environment, as illustrated in Fig. 4. The first two experiments evaluated the fast convergence and tracking accuracy capabilities of the system. In the third experiment, the robustness and adaptability of the system to external disturbances was analyzed. In order to highlight the improvements achieved with our proposed control approach, comparative experiments were performed with a PID controller and a Robust Continuous Sliding Mode Control (RCSMC) [34]. A video demonstrating the experimental results is displayed in https://youtu.be/cfiXpJUivHY. Hereafter, we refer to the base, shoulder, and elbow of the robotic manipulator as $q_1$, $q_2$, and $q_3$, respectively.

**TABLE 2. Physical parameters of the robotic manipulator.**

| Symbol | Definition | Value |
|---|---|---|
| $m_1$ | Base link mass | 4 Kg |
| $m_2$ | Shoulder link mass | 6 Kg |
| $m_3$ | Elbow link mass | 6 Kg |
| $l_1$ | Base link length | 0.1 m |
| $l_2$ | Shoulder link length | 0.3 m |
| $l_3$ | Elbow link length | 0.4 m |
| g | Acceleration of gravity | 9.81 m/s |

**TABLE 3. Control parameters.**

| Parameters | Value |
|---|---|
| $\lambda$ | $\text{diag}(40, 40, 40)$ |
| $\delta$ | $\text{diag}(1.2, 1.2, 1.2)$ |
| $K_0$ | $\text{diag}(12, 12, 12)$ |
| $\eta_0$ | $\text{diag}(0.5, 0.5, 0.5)$ |
| $\alpha_0$ | $\text{diag}(5, 5, 5)$ |
| $\beta_0$ | $\text{diag}(1.5, 1.5, 1.5)$ |

*Remark 4:* It is essential to note that the PID control used in this study for the comparative analysis is considered optimal since the PID control gains were carefully tuned to ensure a satisfactory transient response. Furthermore, this PID control approach represents the controller currently employed by the EOD robotic manipulator. Therefore, one of the main objectives was to improve the existing control method using an advanced nonlinear control approach, as presented in this research.

### 1) EXPERIMENT 1

In this experiment, a time-varying reference trajectory is established for the three joints, which is defined as:

$$q_d = \begin{bmatrix} q_{d1} \\ q_{d2} \\ q_{d3} \end{bmatrix} = \begin{bmatrix} 100 - 29\cos(\frac{t}{1.5\pi}) \\ 120 + 57e^{-0.2t} - (286/20)e^{-0.8t} \\ 100 - 29\cos(\frac{t}{1.5\pi}) \end{bmatrix}. \tag{48}$$

The experimental results are presented in Figs. 5-8. The angular positions and velocities are illustrated in Figs. 5-6, respectively. Fig. 5 shows that the proposed control system ABFTSMC achieves better trajectory tracking capabilities on the three joints of the robotic manipulator in terms of fast convergence in finite time and tracking accuracy compared to the PID and RCSMC controllers. Although the RCSMC control shows interesting results in terms of convergence speed, our proposed control approach exhibits better convergence capabilities and tracking accuracy, which is evident by observing the zoomed regions in Fig. 5. Moreover, both PID and RCSMC control presented difficulties in accurately tracking the trajectory established for the third joint (elbow), a situation that does not occur with our proposed approach, which accurately tracks the reference trajectory. Fig. 7 presents the tracking errors, highlighting that the errors of the proposed control system converge to zero faster and remain in the neighbourhood of the origin. In contrast, the tracking errors of the PID and RCSMC controllers, besides showing a slower convergence rate, do not stay close to the origin, especially in the first and third joints, as shown in Fig. 7. The control inputs of the proposed approach are presented in Fig. 8, showing that the input signals are continuous and chattering-free, which is beneficial for the robotic manipulator in practical EOD applications.

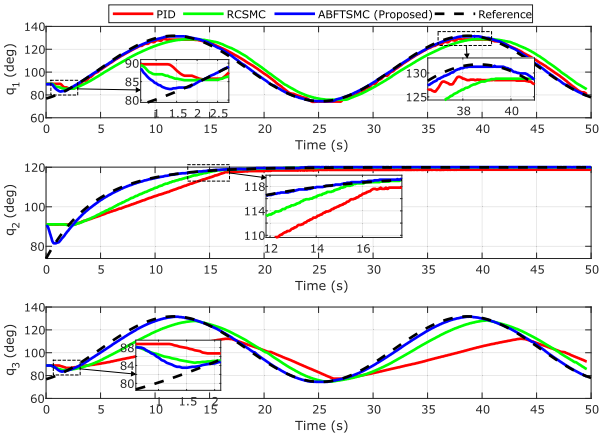


**FIGURE 5. Temporal response of the position of the three joints.**

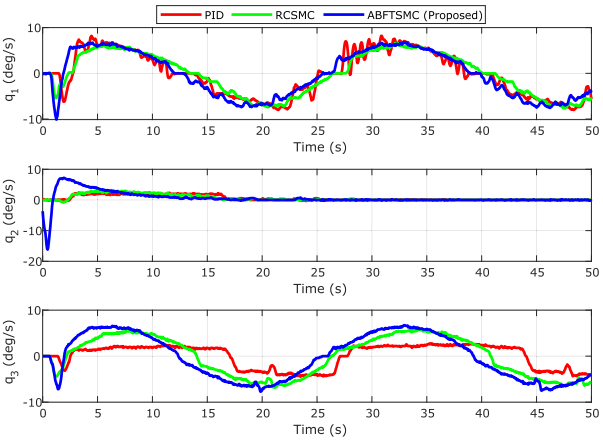


**FIGURE 6. Temporal response of the velocity of the three joints.**

To provide an accurate quantitative comparison of the experimental results and confirm the theoretical findings of

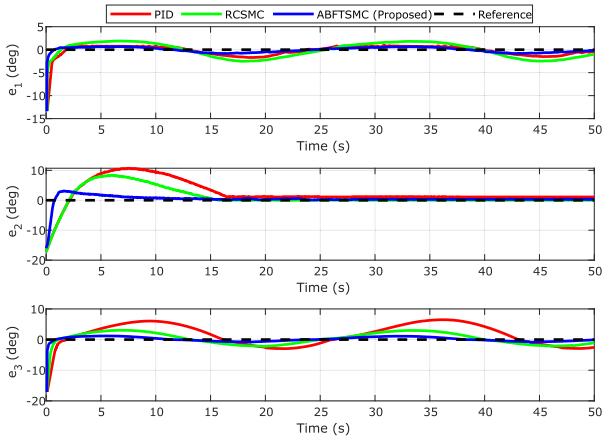


**FIGURE 7.** Temporal response of the tracking errors.

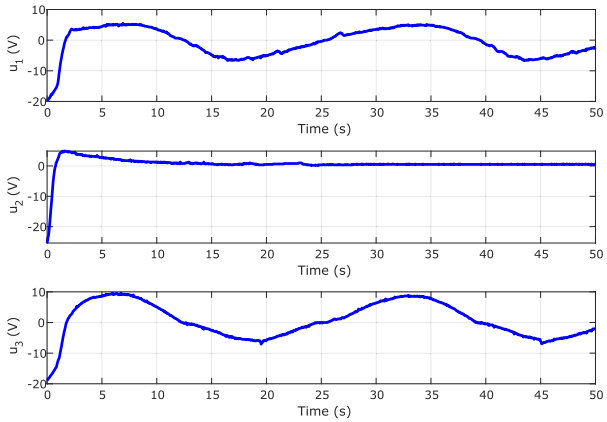


**FIGURE 8.** Control inputs.

the proposed control system, we use the performance indices of settling time, RMSE (Root Mean Square Error), and IAE (Integral Absolute Error) in this research. The settling time is defined as the time it takes for the system errors to converge and stabilize within a range of 2.5% with respect to the origin. RMSE and IAE are metrics to evaluate the performance of the control system in terms of tracking accuracy and are defined as follows:

$$\text{RMSE} = \sqrt{\frac{1}{t_f - t_i}\int_{t_i}^{t_f} e(t)^2\, dt}, \quad \text{IAE} = \int_{t_i}^{t_f} |e(t)|\,, \quad (49)$$

where $t_i$ and $t_f$ represent the initial and final times, respectively. These indices are calculated and presented in Tables 4 and 5, respectively.

**TABLE 4.** Analysis of settling time for experiment 1.

| Control strategy | Settling time | | |
|---|---|---|---|
| | $q_1$ | $q_2$ | $q_3$ |
| PID | 2.011 | 16.06 | 1.546 |
| RCSMC | 1.365 | 14.51 | 1.137 |
| ABFTSMC (proposed) | 0.818 | 2.594 | 0.864 |

**TABLE 5.** Analysis of RMSE and IAE for experiment 1.

| Control | RMSE | | | IAE | | |
|---|---|---|---|---|---|---|
| | $q_1$ | $q_2$ | $q_3$ | $q_1$ | $q_2$ | $q_3$ |
| PID | 4.429 | 4.688 | 12.073 | 14.005 | 14.827 | 38.178 |
| RCSMC | 7.767 | 3.491 | 9.203 | 24.562 | 11.040 | 29.103 |
| ABFTSMC (proposed) | 2.640 | 1.502 | 3.354 | 8.351 | 4.750 | 10.608 |

In Table 4, a quantitative comparison of the settling times of the three controllers is presented. It is observed that our proposed control system, ABFTSMC, has shorter settling times in all three joints of the robotic manipulator compared to PID and RCSMC controllers, which confirms the outstanding feature of the proposed system in terms of fast convergence in finite time. On the other hand, Table 5 shows a quantitative comparison of the RMSE and IAE indices. In this table, it is also clearly observed that our proposed control system, ABFTSMC, presents lower values of RMSE and IAE in the three joints of the robotic manipulator compared to the PID and RCSMC controllers, which confirms the superiority of the proposed system in terms of trajectory tracking accuracy. For better visualization of these results, we plot the information in Table 5 in a bar chart, as shown in Fig. 9.

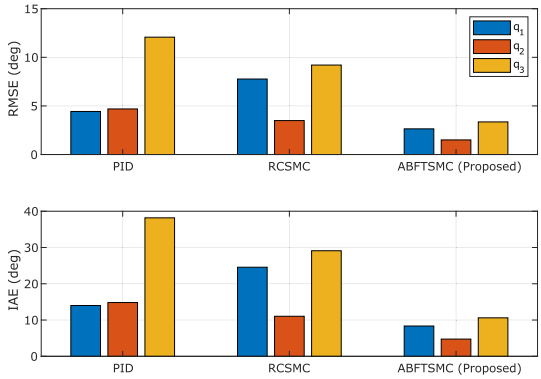


**FIGURE 9.** RMSE and IAE performance index: Experiment 1.

### 2) EXPERIMENT 2

In this experiment, we consider a piece-wise continuous reference trajectory with abrupt changes, as shown in Fig. 10, to highlight the feasibility of the proposed control system. The experimental results are presented in Figs. 10-13. The angular positions and angular velocities are illustrated in Figs. 10-11, respectively. Fig. 10 shows that the proposed control system ABFTSMC achieves fast convergence in finite time at the three joints of the robotic manipulator compared to the PID and RCSMC controllers when abrupt reference changes are applied. Furthermore, by observing the zoomed regions in Fig. 10, it is evident that our proposed control approach achieves high trajectory tracking accuracy in all three joints compared to the other controllers. The tracking

errors for this experiment are presented in Fig. 12, where the errors of the proposed control system converge to zero faster and remain in the neighborhood of the origin compared to the PID and RCSMC controllers, as can be seen in the zoomed regions of Fig. 12. The control inputs of the proposed approach are presented in Fig. 13, showing that the control signals for this experiment are continuous and chattering-free.

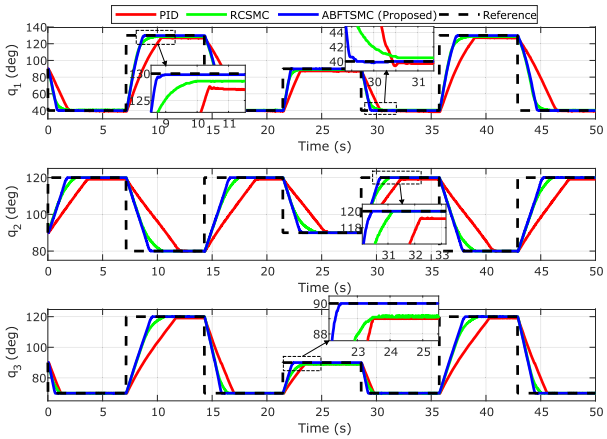


**FIGURE 10.** Temporal response of the position of the three joints.

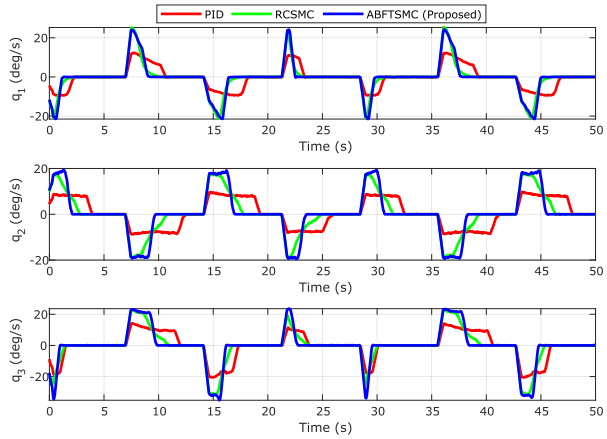


**FIGURE 11.** Temporal response of the velocity of the three joints.

Employing the performance indices described in Experiment 1, they are calculated and presented in Tables 6 and 7, respectively. From Tables 6 and 7, it is highlighted that the proposed control system, ABFTSMC, compared to the PID and RCSMC controllers, has a shorter settling time in the three joints of the robotic manipulator; also, the RMSE and IAE indices of our proposed control approach are lower compared to the other controllers. These experimental results confirm the superiority of the proposed control system in terms of fast convergence in finite time and tracking accuracy compared to the other controllers for continuous part-wise reference trajectories with abrupt changes. In Fig. 14, the error results of Table 7 are illustrated in a bar chart.

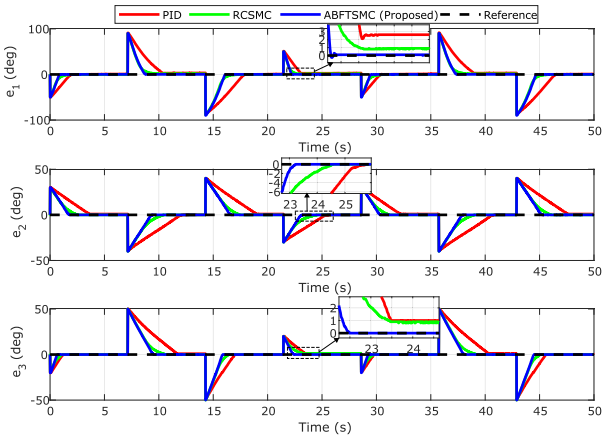


**FIGURE 12.** Temporal response of the tracking errors.

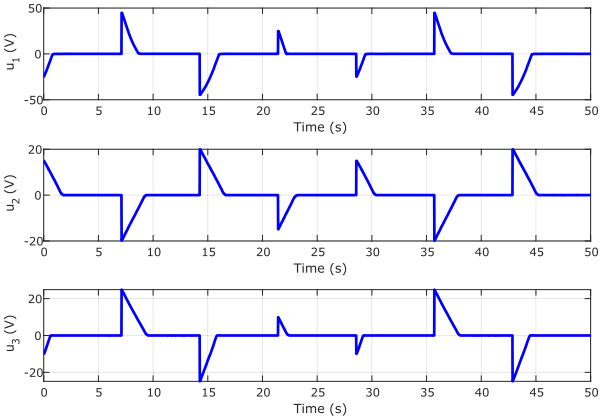


**FIGURE 13.** Control inputs.

**TABLE 6.** Analysis of settling time for experiment 2.

| Control strategy | Settling time | | |
|---|---|---|---|
| | $q_1$ | $q_2$ | $q_3$ |
| PID | 1.931 | 3.910 | 1.229 |
| RCSMC | 1.565 | 2.509 | 1.196 |
| ABFTSMC (proposed) | 0.896 | 1.815 | 0.686 |

**TABLE 7.** Analysis of RMSE and IAE for experiment 2.

| Control | RMSE | | | IAE | | |
|---|---|---|---|---|---|---|
| | $q_1$ | $q_2$ | $q_3$ | $q_1$ | $q_2$ | $q_3$ |
| PID | 5.688 | 3.261 | 3.066 | 17.988 | 10.312 | 9.695 |
| RCSMC | 4.089 | 2.329 | 2.405 | 12.931 | 7.365 | 7.606 |
| ABFTSMC (proposed) | 3.209 | 1.892 | 1.947 | 10.995 | 5.985 | 6.159 |

### 3) EXPERIMENT 3

To demonstrate the effectiveness of the proposed control system ABFTSMC against external disturbances and uncertainties, in this experiment, we incorporate a 10 kg payload to the end effector of the EOD robotic manipulator. This payload simulates a suspect package in real-life scenarios. It is crucial to mention that this payload is considered

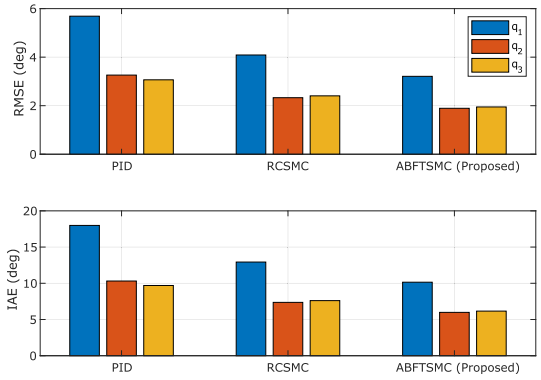


**FIGURE 14.** RMSE and IAE performance index: Experiment 2.

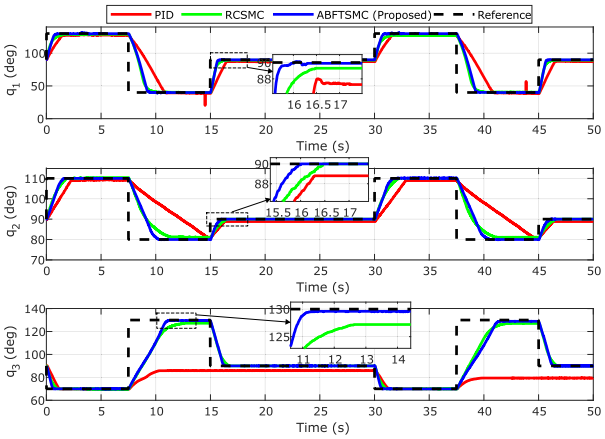


**FIGURE 15.** Temporal response of the position of the three joints.

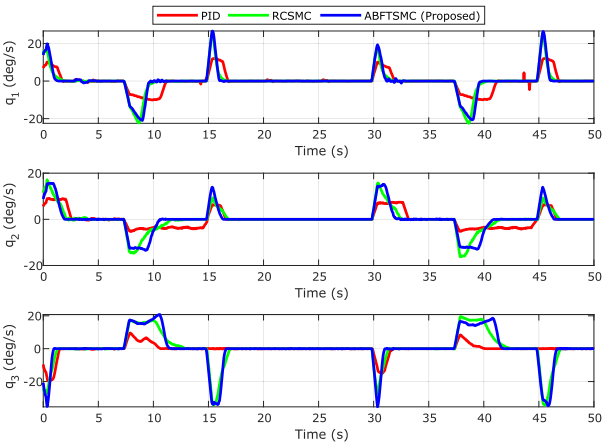


**FIGURE 16.** Temporal response of the velocity of the three joints.

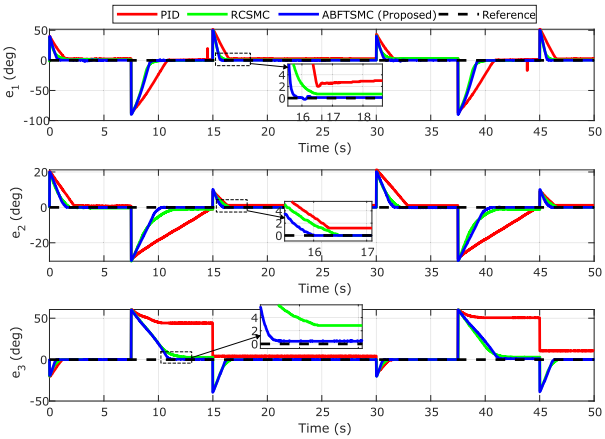


**FIGURE 17.** Temporal response of the tracking errors.

an unknown external disturbance to the control system. Furthermore, a piece-wise continuous reference trajectory with abrupt changes is employed, as shown in Fig. 15.

The experimental results are presented in Figs. 15-18. The angular positions and velocities are illustrated in Figs. 15-16, respectively. Fig. 15 shows that the three joints of the proposed control system ABFTSMC efficiently track the reference trajectory even with the 10 kg payload on the end-effector of the robotic manipulator, demonstrating superior disturbance rejection capability compared to the other controllers. Although the RCSMC approach shows acceptable results, its convergence and accuracy capability are affected by external disturbance, as evidenced in the zoomed regions of Fig. 15. On the other hand, the PID approach is the most affected in this experiment, showing a remarkable sensitivity to external disturbances, especially in the second and third manipulator joints, where the third joint fails to reach the reference trajectory at any time. The tracking errors are shown in Fig. 17, where the errors of the proposed control system efficiently converge to zero and remain in the neighborhood of the origin despite external disturbances and uncertainties. This behavior is attributed to the adaptive neural network scheme, which allows efficient adaptation of the control system to unknown disturbances. Finally, the control inputs for this experiment are presented in Fig. 18, revealing continuous and chattering-free signals, which is beneficial for practical applications of the EOD robotic manipulator.

Fig. 19 presents a sequence of movements at specific times of the robotic manipulator under different implemented controllers. In this figure, the blue dashed line represents the desired setpoint for the third joint of the manipulator, while the green dashed line represents the end-effector position of the robotic manipulator. It is observed that the proposed control system ABFTSMC successfully achieves the desired setpoint smoothly, despite the presence of a 10 kg external disturbance at the end-effector. On the other hand, the RCSMC approach shows acceptable results, although the end-effector does not accurately reach the desired setpoint. In contrast, the PID approach is the most affected since the end effector never reaches the desired setpoint. The experimental results are displayed in the video: https://youtu.be/cfiXpJUivHY.

Tables 8-9 present the calculations obtained from the performance indices described in the previous experiments.

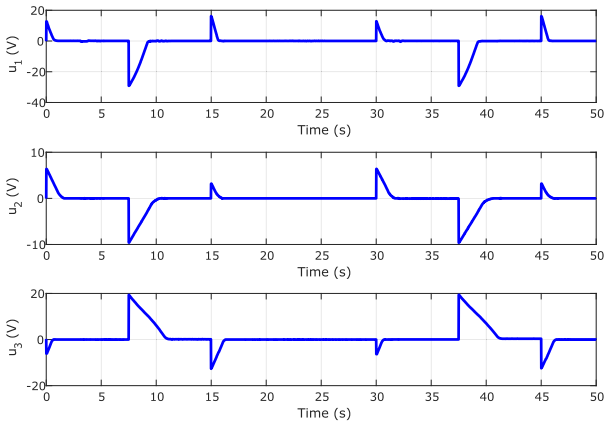


**FIGURE 18.** Control inputs.

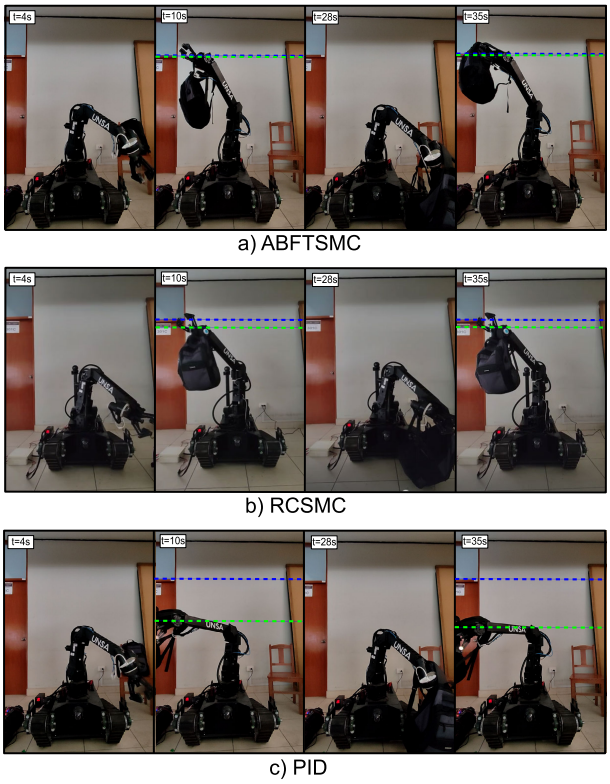


**FIGURE 19.** Sequences of movements of the robotic manipulator for experiment 3. a) Proposed control strategy ABFTSMC. b) RCSMC c) PID control.

The proposed control system ABFTSMC shows a shorter settling time and lower RMSE and IAE indices compared to the PID and RCSMC controllers. These results confirm the superiority of the proposed control system in terms of finite-time convergence, tracking accuracy, and robustness. Fig. 20 illustrates the errors presented in Table 9 using a bar chart.

## VII. LIMITATIONS AND FUTURE WORK

In this research, we have focused on the design, implementation, and experimental validation of a robust nonlinear control system called ABFTSMC for trajectory tracking of an EOD robotic manipulator. However, there are additional aspects that could be addressed in future work, as detailed below:

- Although this research focused on controlling the robotic manipulator joints, neither the direct nor inverse kinematics of the EOD manipulator were addressed. For future work, the ABFTSMC system will be implemented on the direct and inverse kinematics of the manipulator, which will allow the planning of position targets through joint movements to achieve those targets.
- The proposed control system has not yet been integrated with interfaces that facilitate human-robot interaction with the robotic manipulator for EOD manipulation tasks. For future work, the ABFTSMC system will be integrated with multimodal interfaces such as haptic, gesture-based, and virtual reality interfaces. These interfaces require fast response, high accuracy, and robustness of the robotic manipulator, which have been achieved in this experimental work.

**TABLE 8.** Analysis of settling time for experiment 3.

| Control strategy | Settling time | | |
|---|---|---|---|
| | $q_1$ | $q_2$ | $q_3$ |
| PID | 1.976 | 2.664 | – |
| RCSMC | 1.663 | 1.934 | 1.121 |
| ABFTSMC (proposed) | 0.963 | 1.613 | 0.662 |

**TABLE 9.** Analysis of RMSE and IAE for experiment 3.

| Control | RMSE | | | IAE | | |
|---|---|---|---|---|---|---|
| | $q_1$ | $q_2$ | $q_3$ | $q_1$ | $q_2$ | $q_3$ |
| PID | 4.337 | 2.178 | 5.481 | 13.717 | 6.889 | 17.333 |
| RCSMC | 3.141 | 1.346 | 2.842 | 9.934 | 4.258 | 8.988 |
| ABFTSMC (proposed) | 2.531 | 1.142 | 2.423 | 8.006 | 3.612 | 7.664 |

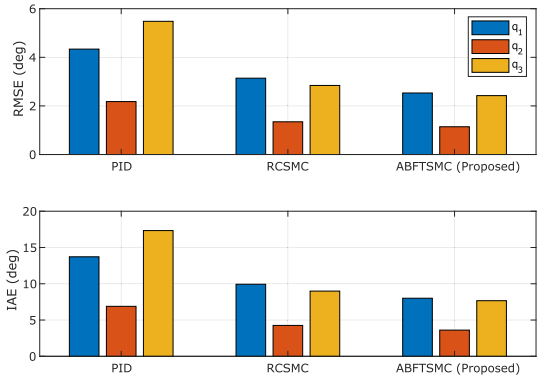


**FIGURE 20.** RMSE and IAE performance index: Experiment 3.

## VIII. CONCLUSION

This article has comprehensively addressed the theoretical design, practical implementation, and experimental validation of a robust finite-time advanced control system for trajectory tracking in an EOD robotic manipulator. Backstepping and Sliding Mode nonlinear control theories were combined along with an adaptive neural network

scheme to develop the ABFTSMC strategy. The control approach developed in this research leads to finite time convergence of all states of the robotic manipulator to the reference signals. Moreover, the proposed approach proved insensitive to external disturbances and uncertainties.

Several experimental tests were performed on a real robotic manipulator to validate the theoretical findings of the proposed control system ABFTSMC. A comparative study with a linear control PID and an advanced control RCSMC was also carried out. The results of these experiments, supported by a quantitative comparative analysis, clearly evidence the effectiveness and superiority of the proposed control system in terms of fast convergence in finite time, high trajectory tracking accuracy, and robustness, which positions it as a promising solution for EOD robotic manipulator control.

## REFERENCES

[1] Y. Gao and F. Wang, *Advanced Studies of Flexible Robotic Manipulators: Modeling, Design, Control and Applications*. Singapore: World Scientific, 2003.
[2] L. Tsai, *Robot Analysis: The Mechanics of Serial and Parallel Manipulators*. Hoboken, NJ, USA: Wiley, 1999.
[3] M. Blatnický, J. Dižo, J. Gerlici, M. Sága, T. Lack, and E. Kuba, "Design of a robotic manipulator for handling products of automotive industry," *Int. J. Adv. Robotic Syst.*, vol. 17, no. 1, Jan. 2020, Art. no. 172988142090629.
[4] H. N. Ghafil and K. Jármai, "Research and application of industrial robot manipulators in vehicle and automotive engineering, a survey," in *Proc. Vehicle Automot. Eng.*, Miskolc, Hungary, 2018, pp. 611–623.
[5] I. Nisky, A. M. Okamura, and M. H. Hsieh, "Effects of robotic manipulators on movements of novices and surgeons," *Surgical Endoscopy*, vol. 28, no. 7, pp. 2145–2158, Jul. 2014.
[6] M. H. Korayem and V. Vahidifar, "Detecting hand's tremor using leap motion controller in guiding surgical robot arms and laparoscopic scissors," *Measurement*, vol. 204, Nov. 2022, Art. no. 112133.
[7] J. Trevelyan, W. R. Hamel, and S. C. Kang, "Robotics in hazardous applications," in *Springer Handbook of Robotics*. Berlin, Germany: Springer, 2016, pp. 1521–1548.
[8] B. Lacevic, P. Rocco, and A. M. Zanchettin, "Safety assessment and control of robotic manipulators using danger field," *IEEE Trans. Robot.*, vol. 29, no. 5, pp. 1257–1270, Oct. 2013.
[9] J. G. Mamani, P. Pinto, D. V. Goyzueta, E. S. Colquehuanca, E. S. Espinoza, and Y. S. Vidal, "Compilation and analysis of requirements for the design of an explosive ordnance disposal robot prototype applied in UDEX-arequipa," in *Proc. Int. Conf. Human-Comput. Interact.*, 2021, pp. 131–138.
[10] C. Xiao, A. B. Woeppel, G. M. Clepper, S. Gao, S. Xu, J. F. Rueschen, D. Kruse, W. Wu, H. Z. Tan, T. Low, S. P. Beaudoin, B. W. Boudouris, W. G. Haris, and J. P. Wachs, "Tactile and chemical sensing with haptic feedback for a telepresence explosive ordnance disposal robot," *IEEE Trans. Robot.*, vol. 39, no. 5, pp. 3368–3381, Jun. 2023.
[11] D. V. Goyzueta, M. J. Guevara, A. A. Montoya, E. E. Sulla, and S. Y. Lester, "Analysis of a user interface based on multimodal interaction to control a robotic arm for EOD applications," *Electronics*, vol. 11, no. 11, p. 1690, May 2022.
[12] A. M. Angulo, L. P. Pinto, E. S. Espinoza, Y. S. Vidal, and E. S. Colquehuanca, "Assisted operation of a robotic arm based on stereo vision for positioning near an explosive device," *Robotics*, vol. 11, no. 5, p. 100, Sep. 2022.
[13] N. O. M. Chilo, L. F. C. Ccari, E. Supo, E. S. Espinoza, Y. S. Vidal, and L. Pari, "Optimal signal processing for steady control of a robotic arm suppressing hand tremors for EOD applications," *IEEE Access*, vol. 11, pp. 13163–13178, 2023.
[14] A. Stefan, L. S. Grigore, I. Oncioiu, D. Constantin, S. Mustata, V. F. Toma, C. Molder, and D. Gorgoteanu, "Influence of the stiffness of the robotic arm on the position of the effector of an EOD robot," *Electronics*, vol. 11, no. 15, p. 2355, Jul. 2022.
[15] L. Sciavicco and B. Siciliano, *Modelling and Control of Robot Manipulators*. Berlin, Germany: Springer, 2001.
[16] D. Zhang and B. Wei, "A review on model reference adaptive control of robotic manipulators," *Annu. Rev. Control*, vol. 43, pp. 188–198, Jan. 2017.
[17] N. Adhikary and C. Mahanta, "Sliding mode control of position commanded robot manipulators," *Control Eng. Pract.*, vol. 81, pp. 183–198, Dec. 2018.
[18] R. Sharma, K. P. S. Rana, and V. Kumar, "Performance analysis of fractional order fuzzy PID controllers applied to a robotic manipulator," *Exp. Syst. Appl.*, vol. 41, no. 9, pp. 4274–4289, Jul. 2014.
[19] H. V. H. Ayala and L. D. S. Coelho, "Tuning of PID controller based on a multiobjective genetic algorithm applied to a robotic manipulator," *Exp. Syst. Appl.*, vol. 39, no. 10, pp. 8968–8974, Aug. 2012.
[20] P. R. Ouyang, W. J. Zhang, and M. M. Gupta, "An adaptive switching learning control method for trajectory tracking of robot manipulators," *Mechatronics*, vol. 16, pp. 51–61, Feb. 2006.
[21] P. Van Cuong and W. Y. Nan, "Adaptive trajectory tracking neural network control with robust compensator for robot manipulators," *Neural Comput. Appl.*, vol. 27, no. 2, pp. 525–536, Feb. 2016.
[22] R.-J. Wai and P.-C. Chen, "Intelligent tracking control for robot manipulator including actuator dynamics via TSK-type fuzzy neural network," *IEEE Trans. Fuzzy Syst.*, vol. 12, no. 4, pp. 552–559, Aug. 2004.
[23] C. Van Pham and Y. N. Wang, "Robust adaptive trajectory tracking sliding mode control based on neural networks for cleaning and detecting robot manipulators," *J. Intell. Robotic Syst.*, vol. 79, no. 1, pp. 101–114, Jul. 2015.
[24] Q. Hu, L. Xu, and A. Zhang, "Adaptive backstepping trajectory tracking control of robot manipulator," *J. Franklin Inst.*, vol. 349, no. 3, pp. 1087–1105, Apr. 2012.
[25] N. Nikdel, M. A. Badamchizadeh, V. Azimirad, and M. A. Nazari, "Adaptive backstepping control for an n-degree of freedom robotic manipulator based on combined state augmentation," *Robot. Comput.-Integr. Manuf.*, vol. 44, pp. 129–143, Apr. 2017.
[26] S. Yu, X. Yu, B. Shirinzadeh, and Z. Man, "Continuous finite-time control for robotic manipulators with terminal sliding mode," *Automatica*, vol. 41, no. 11, pp. 1957–1964, Nov. 2005.
[27] Y. Feng, X. Yu, and Z. Man, "Non-singular terminal sliding mode control of rigid manipulators," *Automatica*, vol. 38, no. 12, pp. 2159–2167, Dec. 2002.
[28] L. F. C. Ccari and P. R. Yanyachi, "A novel neural network-based robust adaptive formation control for cooperative transport of a payload using two underactuated quadcopters," *IEEE Access*, vol. 11, pp. 36015–36028, 2023.
[29] O. Mechali, L. Xu, Y. Huang, M. Shi, and X. Xie, "Observer-based fixed-time continuous nonsingular terminal sliding mode control of quadrotor aircraft under uncertainties and disturbances for robust trajectory tracking: Theory and experiment," *Control Eng. Pract.*, vol. 111, Jun. 2021, Art. no. 104806.
[30] N. K. Goswami and P. K. Padhy, "Sliding mode controller design for trajectory tracking of a non-holonomic mobile robot with disturbance," *Comput. Electr. Eng.*, vol. 72, pp. 307–323, Nov. 2018.
[31] O. Mechali, L. Xu, X. Xie, and J. Iqbal, "Fixed-time nonlinear homogeneous sliding mode approach for robust tracking control of multirotor aircraft: Experimental validation," *J. Franklin Inst.*, vol. 359, no. 5, pp. 1971–2029, Mar. 2022.
[32] X. Yin, L. Pan, and S. Cai, "Robust adaptive fuzzy sliding mode trajectory tracking control for serial robotic manipulators," *Robot. Comput.-Integr. Manuf.*, vol. 72, Dec. 2021, Art. no. 101884.
[33] S.-H. Han, M. S. Tran, and D.-T. Tran, "Adaptive sliding mode control for a robotic manipulator with unknown friction and unknown control direction," *Appl. Sci.*, vol. 11, no. 9, p. 3919, Apr. 2021.
[34] J. Xian, L. Shen, J. Chen, and W. Feng, "Continuous sliding mode control of robotic manipulators based on time-varying disturbance estimation and compensation," *IEEE Access*, vol. 10, pp. 43473–43480, 2022.
[35] S. Mondal and C. Mahanta, "Adaptive second order terminal sliding mode controller for robotic manipulators," *J. Franklin Inst.*, vol. 351, no. 4, pp. 2356–2377, Apr. 2014.
[36] N. Kumar, "Finite time control scheme for robot manipulators using fast terminal sliding mode control and RBFNN," *Int. J. Dyn. Control*, vol. 7, no. 2, pp. 758–766, Jun. 2019.
[37] K. S. Chaudhary and N. Kumar, "Fractional order fast terminal sliding mode control scheme for tracking control of robot manipulators," *ISA Trans.*, vol. 142, pp. 57–69, Nov. 2023.

[38] Z. Chen, X. Yang, and X. Liu, "RBFNN-based nonsingular fast terminal sliding mode control for robotic manipulators including actuator dynamics," *Neurocomputing*, vol. 362, pp. 72–82, Oct. 2019.
[39] S. Yi and J. Zhai, "Adaptive second-order fast nonsingular terminal sliding mode control for robotic manipulators," *ISA Trans.*, vol. 90, pp. 41–51, Jul. 2019.
[40] M. Hong, X. Gu, L. Liu, and Y. Guo, "Finite time extended state observer based nonsingular fast terminal sliding mode control of flexible-joint manipulators with unknown disturbance," *J. Franklin Inst.*, vol. 360, no. 1, pp. 18–37, Jan. 2023.
[41] Z. Dachang, D. Baolin, Z. Puchen, and W. Wu, "Adaptive backstepping sliding mode control of trajectory tracking for robotic manipulators," *Complexity*, vol. 2020, pp. 1–11, Aug. 2020.
[42] T. N. Truong, A. T. Vo, and H.-J. Kang, "A backstepping global fast terminal sliding mode control for trajectory tracking control of industrial robotic manipulators," *IEEE Access*, vol. 9, pp. 31921–31931, 2021.
[43] M. Vijay and D. Jena, "Backstepping terminal sliding mode control of robot manipulator using radial basis functional neural networks," *Comput. Electr. Eng.*, vol. 67, pp. 690–707, Apr. 2018.
[44] J. Baek and M. Kang, "A practical adaptive sliding-mode control for extended trajectory-tracking of articulated robot manipulators," *IEEE Access*, vol. 10, pp. 116907–116918, 2022.
[45] J. Baek, M. Jin, and S. Han, "A new adaptive sliding-mode control scheme for application to robot manipulators," *IEEE Trans. Ind. Electron.*, vol. 63, no. 6, pp. 3628–3637, Jun. 2016.
[46] L. Bao, D. Kim, S.-J. Yi, and J. Lee, "Design of a sliding mode controller with fuzzy rules for a 4-DoF service robot," *Int. J. Control, Autom. Syst.*, vol. 19, no. 8, pp. 2869–2881, Aug. 2021.
[47] A. Q. Al-Dujaili, A. Falah, A. J. Humaidi, D. A. Pereira, and I. K. Ibraheem, "Optimal super-twisting sliding mode control design of robot manipulator: Design and comparison study," *Int. J. Adv. Robotic Syst.*, vol. 17, no. 6, Nov. 2020, Art. no. 172988142098152.
[48] J. Zhao, T. Han, X. Ma, W. Ma, C. Liu, J. Li, and Y. Liu, "Research on kinematics analysis and trajectory planning of novel EOD manipulator," *Appl. Sci.*, vol. 11, no. 20, p. 9438, Oct. 2021.
[49] L. A. Zuniga A., J. C. Pedraza O., E. Gorrostieta, L. Garcia-Valdovinos, J. M. Ramos, and C. A. Gonzalez, "Design and manufacture of a mobile robot applied to the manipulation of explosives," in *Proc. 11th IEEE Int. Power Electron. Congr.*, Aug. 2008, pp. 84–89.
[50] S. Deng, H. Cai, K. Li, Y. Cheng, Y. Ni, and Y. Wang, "The design and analysis of a light explosive ordnance disposal manipulator," in *Proc. 2nd Int. Conf. Robot. Autom. Sci. (ICRAS)*, Jun. 2018, pp. 1–5.
[51] N. Ahmad, F. M. Malik, S. Hussain, and O. Altaf, "Design of adaptive SMC for EOD robotics manipulator arm," in *Proc. Int. Conf. Control, Dyn. Syst., Robot.*, Jun. 2018, pp. 1–8.
[52] L. Wang, T. Chai, and L. Zhai, "Neural-network-based terminal sliding-mode control of robotic manipulators including actuator dynamics," *IEEE Trans. Ind. Electron.*, vol. 56, no. 9, pp. 3296–3304, Sep. 2009.
[53] F. Wang, B. Chen, X. Liu, and C. Lin, "Finite-time adaptive fuzzy tracking control design for nonlinear systems," *IEEE Trans. Fuzzy Syst.*, vol. 26, no. 3, pp. 1207–1216, Jun. 2018.
[54] H. J. Brascamp and E. H. Lieb, "Best constants in Young's inequality, its converse, and its generalization to more than three functions," *Adv. Math.*, vol. 20, no. 2, pp. 151–173, May 1976.
[55] N.-N. Zhao, L.-B. Wu, X.-Y. Ouyang, Y. Yan, and R.-Y. Zhang, "Finite-time adaptive fuzzy tracking control for nonlinear systems with disturbances and dead-zone nonlinearities," *Appl. Math. Comput.*, vol. 362, Dec. 2019, Art. no. 124494.
[56] J. Liu, X. Wang, J. Liu, and X. Wang, *Advanced Sliding Mode Control*. Berlin, Germany: Springer, 2011.
[57] T. D. C. Thanh and K. K. Ahn, "Nonlinear PID control to improve the control performance of 2 axes pneumatic artificial muscle manipulator using neural network," *Mechatronics*, vol. 16, no. 9, pp. 577–587, Nov. 2006.
[58] H. Razmi and S. Afshinfar, "Neural network-based adaptive sliding mode control design for position and attitude control of a quadrotor UAV," *Aerosp. Sci. Technol.*, vol. 91, pp. 12–27, Aug. 2019.
[59] R. Murray, Z. Li, and S. Sastry, *A Mathematical Introduction to Robotic Manipulation*. Boca Raton, FL, USA: CRC Press, 2017.
[60] A. Senatore and G. Ventura, "Sliding mode control design for EOD robot manipulator and multiphysic analysis," in *Proc. 26th Int. Conf. Mechatronics Technol. (ICMT)*, Oct. 2023, pp. 1–5.

**LUIS F. CANAZA CCARI** received the B.Sc. degree in electronic engineering from the Universidad Nacional de San Agustín (UNSA) of Arequipa, Peru, in 2021. Between 2022 and 2023, he worked as a Research Assistant in the project "Design and Development of an EOD Robot with Multimodal Control Interface," funded by CONCYTEC—Peru. He is a RENACYT Researcher certified by CONCYTEC. He is currently a Research Assistant at the Institute IAAPP—UNSA. His research interests include autonomous robotics, advanced nonlinear control, system modeling, control of quadcopters, robotic manipulators, and multi-agent systems.

**WALKER AGUILAR** received the B.S. degree in electronic engineering from the National University of San Agustin of Arequipa, Peru, in 2023. His expertise extends as a Hardware Developer for startups in Peru, offering innovative solutions. He is currently a Research Assistant at UNSA in the project "Design and Development of an EOD robot with Multimodal Control Interface"—CONCYTEC. His research interests include robotics and hardware.

**ELVIS SUPO** is a RENACYT Researcher. He is a specialist in project management and has experience advising and directing 15 applied research projects. His research interests include biomedical engineering and robotics.

**ERASMO SULLA ESPINOZA** received the B.S. and M.S. degrees in electronic engineering from Universidad Nacional de San Agustín de Arequipa, in 1994 and 2013, respectively, where he is currently pursuing the Ph.D. degree in mechatronics engineering. He is a Principal Professor of biomedical engineering with Universidad Nacional de San Agustín de Arequipa.

**NICOLÁS MEDINA** was born in Cusco, Peru, in 1998. He received the Engineering degree in electronic engineering from Universidad Nacional de San Agustín de Arequipa (UNSA), in 2024. He is currently a Researcher with the Project "Design and Development of an EOD Robot With Multimodal Control Interface"—CONCYTEC. His research interests include NUI and multimodal interfaces, unmanned vehicles, robotics, and biomedical engineering.

**LIZARDO PARI** received the B.S. and M.S. degrees in electronic engineering from Universidad Nacional de San Agustín de Arequipa, Peru, in 1996 and 2005, respectively, and the Ph.D. degree in automation and robotics from the Polytechnic University of Madrid, Spain, in 2007. He is currently a Principal Professor and the Head of the Vision and Robotics Group, Universidad Nacional de San Agustín de Arequipa. His research interests include computer vision, motion tracking, three-dimensional reconstruction, and visual control. He was a member of the IEEE Robotics and Automation Society Peru Section.